# Paleoclimatic reconstructions based on borehole temperature measurements in ice sheets. Possibilities and limitations

Andrey N. Salamatin

Department of Applied Mathematics, Kazan State University, 18, Kremlyevskaya Street, Kazan 420008, RUSSIA

**Abstract:** This paper revises recent studies [1–7] on paleoclimatic reconstructions from borehole thermometry at Vostok (East Antarctica), using more precise or complete, ice-core and environmental data. The principles of a model for heat transfer and ice flow are described. Three sequential possible steps of data processing are considered: 1) inverse reconstruction of the dominant (metronomic) part of the past orbitally driven temperature variations on the glacier surface from the borehole temperature profile; 2) correlation of the main climatic events on the smoothed ice-core isotope record with those on the geophysical metronome resulting in the ice age – depth relationship; 3) calibration of the transfer function converting the isotopic content measurements to past surface temperatures. Glaciological and paleoclimatological implications of the results are discussed.

## 1. Introduction

Different properties of ice cores are indicators of past climatic changes. Among them, isotope records are recognized as the most direct proxy signals of the paleo-temperature variations. Their quantitative interpretation encounters two problems: 1) ice-core age dating and 2) paleothermometer calibration. Traditional approaches based on modelling ice-sheet dynamics and measuring geographical isotope-temperature slopes still allow a significant level of uncertainty, and paleoreconstructions require additional independent sources of related data to become more reliable.

From this point of view borehole temperature profiles could provide another piece of relevant information. Certainly, the value of such paleosignals is limited because of their low resolution and comparatively short memory. Numerous studies show that only the recent 10–20 kyear history of smoothed surface temperature variations can be straightforwardly distinguished in the temperature-depth curve from a large ice sheet. Thus, mathematically, any inverse procedure of long-term and/or detailed paleotemperature reconstructions from borehole temperature measurements should be formulated as a solution to an ill-stated problem. This means that strict *a priori* constraints must be imposed on the permissible parametric form of initial temperature conditions and past temperature variations. The choice of these constraints is the key step which predetermines the possibility and success of using borehole

*Physics of Ice Core Records*
Edited by T. Hondoh
Hokkaido University Press, 2000, Sapporo

temperature profiles in paleoclimatic reconstructions. The central part of Antarctic Plateau with its minimal precipitation rates and maximal ice thickness and age is a unique place on Earth, where the present-day ice-sheet temperature is influenced by at least the recent 50–100 kyear climatic changes. Hence the dominant "metronomic" component of the local surface temperature history can be deduced under the basic (*a priori*) assumption that Milankovich astronomic cycles prevailed in the Pleistocene climate. The correlation of peaks and troughs of the metronomic signal with those on the smoothed isotope record leads to the ice-core timescale. The transfer function between the isotope record and the surface temperature variations can also be constrained by minimizing the mean-square deviation between the borehole temperature measurements and model predictions.

The paper is mainly built on research results [1–7] obtained during the recent ten years (1989–1998) and is an attempt to incorporate the borehole thermometry data into ice-core analysis and paleoclimatic reconstructions within the framework of the Deep Drilling Project at Vostok Station (East Antarctica). However, it should not be considered as a mere review. Most of the simulations are newly performed with recent data that are more precise or complete. The principal aim of the study is to reveal possibilities and to point out limitations, related to the use of the ice-sheet temperature memory, and also to emphasize the uniqueness of central Antarctica, particularly Vostok, for this analysis. Pursuing the above goals and plans, we can not go deep into discussion of mathematical methods used in this study and into its theoretical background, although relevant and sufficient references are included. We also leave necessary additional comments to the following sections and start with a description of a mathematical model for the heat transfer and ice flow in a central part of a large ice sheet, with a special reference to the conditions in the Vostok region.

## 2. Mathematical model

### 2.1. Heat transfer equation

To decipher the information about the climate history preserved in a present-day temperature profile, one needs first a mathematical model which would relate the climatic input to the evolution of the glacier temperature field $T$ in time $t$. The conventional heat transfer equation along a fixed ice-flow line in the shallow-ice approximation [8, 9] takes the form:

$$\rho c\left(\frac{\partial T}{\partial t}+u\frac{\partial T}{\partial s}+w\frac{\partial T}{\partial z}\right)=\frac{\partial}{\partial z}\left(\lambda\Lambda\frac{\partial T}{\partial z}\right)+Q. \tag{1}$$

Here $s$ is the distance from the ice divide along the reference flow line and $z$ is the vertical coordinate with the $z$-axis directed upward (see Fig. 1); $u$ and $w$ are the longitudinal and vertical velocities respectively; $Q$ is the strain heating; $\rho$ is the density of snow-firn-ice deposits; $c$ and $\lambda$ are the specific heat and thermal conductivity of pure ice respectively, while $\Lambda$ is the thermal-conductivity correction factor which accounts for the enhanced thermal resistance of the porous ice structure.

Due to the snow-to-ice transformation, the density and thermal conductivity of the upper glacier strata vary significantly with depth, $h = l–z$, measured from the ice-sheet

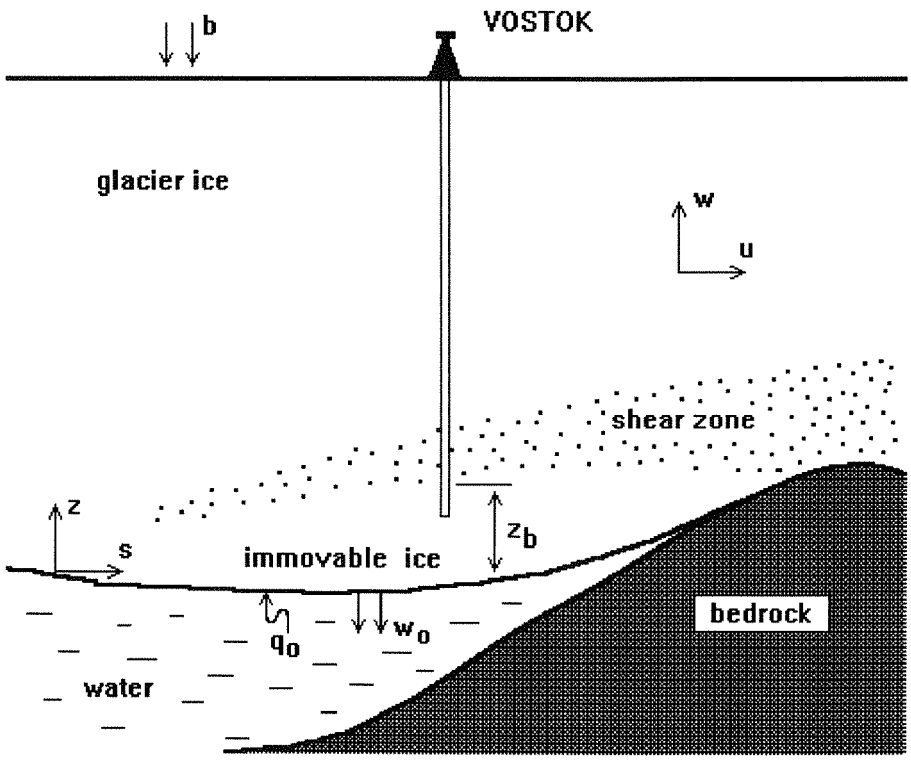


Figure 1: A schematic picture of the ice-sheet flow in the vicinities of Vostok Station with the principal characteristics. The basal ice flow may be dammed by the bedrock rise at the edge of the subglacial lake downstream from Vostok and two limiting cases have to be considered: (I) shear deformation and strain heating in the 3540-meter stratum of the ice sheet overlying the immovable ice and (II) no shear in the freely floating ice.

surface elevation $l(s, t)$. Hence, in general, we write

$$\rho = \rho_0 \bar{\rho}(h), \quad c = c_0 \bar{c}(T), \quad \lambda = \lambda_0 \bar{\lambda}(T),$$
$$\Lambda = \Lambda(\bar{\rho}), \qquad (2)$$

where the overbarred values are the relative characteristics normalized by the typical properties of pure ice designated by the subscript "$_0$".

Physical properties of ice and other model parameters are presented in Table 1 together with their basic values assumed for simulations in Vostok Station area.

The density profile is determined after Lipenkov et al. [10]. Thermophysical characteristics of pure ice are taken as in [4, 6] in accordance with Hobbs [11] and Vostretsov et al. [12]. A Maxwell type formula for $\Lambda(\bar{\rho})$ approximates the measurements by Vostretsov et al. [12] and the wide set of data for snow and firn collected by Sturm et al. [13].

### 2.2. Ice flow and compressibility effects

Eq. 1 should be coupled with an ice-flow model for the velocity field $u$, $w$ and the strain heating $Q$. This question was specially addressed in [2] to extend the theory of the flow-line modelling and shallow-ice

Table 1: Heat transfer and ice-flow model parameters for Vostok Station.

| Meaning of parameters | Denotations | Basic values* and formulas |
|---|---|---|
| *Environmental conditions:* | | |
| Inversion temperature | $T_i$ | $T_i^0 = -39°C$ |
| Ice-equivalent thickness | $\Delta$ | $\Delta^0 = 3740$ m |
| Mass balance | $b$ | $b^0 = 2.4$ cm/yr |
| Exponent factor of mass-balance variations | $\eta_b$ | $6148.3/(273.15 + T_i^0)^2$, $0.112°C^{-1}$ |
| Relative mass-balance excess | $e_b$ | 0.25 |
| Shear-flow-rate ratio | $\sigma$ | 1 (case I) and 0 (case II) |
| Basal-shear level | $z_b$ | 230 m |
| *Physical properties of glacier ice:* | | |
| Density of snow-firn-ice deposits | $\rho$ | $\rho_0\left(1 - c_s e^{-\gamma_s h}\right)$, $\rho_0 = 920$ kg·m$^{-3}$, $c_s = 0.69$, $\gamma_s = 0.021$ m$^{-1}$ |
| Specific heat capacity of ice | $c(T)$ | $c_0[1 + \alpha_c(T + 30)]$, $c_0 = 1.88$ kJ·(kg·°C)$^{-1}$, $\alpha_c = 0.004°C^{-1}$ |
| Thermal conductivity of ice | $\lambda(T)$ | $\lambda_0\left[1 - \alpha_\lambda(T + 30)\right]$, $\lambda_0 = 2.55$ W·(m·°C)$^{-1}$, $\alpha_\lambda = 0.0044°C^{-1}$ |
| Relative thermal conductivity of porous (snow-firn) ice structure | $\Lambda(\bar{\rho})$ | $\left(\beta_\lambda \bar{\rho}\right)/\left(\beta_\lambda + 1 - \bar{\rho}\right)$, $\beta_\lambda = 0.5$ |
| Surface heat transfer coefficient | $\chi$ | $\frac{1}{\gamma_s}\left[c_s - \frac{\beta_\lambda + 1}{\beta_\lambda}\ln(1 - c_s)\right]$, 200 m |
| Latent heat of fusion | $L_f$ | 333 kJ·kg$^{-1}$ |
| Glen-flow-law exponent | $\alpha$ | 3.0 |
| *Tuning parameters* | | |
| Non-isothermal-flow exponent | $\beta$ | 10 |
| Mass-balance amplification factor | $\gamma_b$ | 0.56 |
| Ice-sheet growth feed-back factor | $\gamma_l$ | 2.53 |
| Relative scale of ice thickness | $K_l$ | 0.57 |
| Reduced site location | $\bar{s}_d$ | 0.1 |

*) Here superscript "0" denotes the present-day values of characteristics

approximation in order to account for the compressibility of the near-surface glacier strata.

Velocity profiles were obtained in terms of the reduced vertical distance $\zeta$ measured as equivalent thickness of pure ice from the glacier bottom relief $z_0(s, t)$ and normalized by the local current ice-equivalent thickness $\Delta(s, t)$:

$$\zeta = \frac{1}{\Delta}\int_{z_0}^{z} \overline{\rho} dz\,, \quad \Delta = \int_{z_0}^{l} \overline{\rho} dz\,. \tag{3}$$

Let $A(s, t)$ designate the total ice-flow rate along the reference flow tube normalized by the tube width $H(s)$:

$$A = \frac{1}{H}\int_0^s \left(b - w_0 - \frac{\partial \Delta}{\partial t}\right) H ds\,, \tag{4}$$

where $b$ is the ice mass balance (accumulation rate) on the free surface and $w_0$ is the ice melting rate at the bottom of the ice sheet.

Let us also introduce the tuning parameter $\sigma$ ($0 \le \sigma \le 1$) as a ratio between the partial ice-flow rate due to the shear strains and the quantity $A$, which includes ice sliding at the bottom, so that the sliding velocity is $u_0 = (1-\sigma)A/\Delta$.

For Glen's flow law, $2e_0 = \tau_0^{\alpha}/\mu(T)$, which relates the effective strain rate $e_0$ and stress $\tau_0$ in the glacier body ($\alpha$ is the creep exponent and $\mu$ is the temperature dependent viscosity factor), we write after Salamatin [2]:

$$\sigma|A| = (g\rho_0)^{\alpha} \Delta^{\alpha+2} \left|\frac{\partial l}{\partial s}\right|^{\alpha} \int_0^1 \frac{(1-\xi)^{\alpha+1}}{\mu} d\xi\,;$$

$$u = \frac{A}{\Delta}\left[1 - \sigma(1-G)\right],$$

$$G(\zeta) = \int_0^{\zeta} \frac{(1-\xi)^{\alpha}}{\mu} d\xi \Big/ \int_0^1 \frac{(1-\xi)^{\alpha+1}}{\mu} d\xi\,; \tag{5}$$

$$\overline{\rho} w = -b + \frac{\partial l}{\partial t} + (1-\zeta)\left(b - w_0 - \frac{\partial \Delta}{\partial t}\right)\left[1 + \sigma\left(\frac{1-F}{1-\zeta}\right) - 1\right] + \left(\frac{\partial z_0}{\partial s} + \zeta \frac{\partial \Delta}{\partial s}\right) u - \left(1 - \overline{\rho}\right)\left(\frac{\partial l}{\partial t} + u \frac{\partial l}{\partial s}\right) + (1-\zeta) A \frac{\partial}{\partial s}\left[\sigma\left(\frac{1-F}{1-\zeta} - 1\right)\right],$$

$$F(\zeta) = \int_0^{\zeta} \frac{(\zeta - \xi)(1-\xi)^{\alpha}}{\mu} d\xi \Big/ \int_0^1 \frac{(1-\xi)^{\alpha+1}}{\mu} d\xi\,.$$

Here $s$ and $\zeta$ are considered as independent variables and $g$ is the gravitational acceleration. The integrals $G$ and $F$ are functions of $\zeta$ and describe the vertical profiles of ice velocity in the glacier. The dependence on the longitudinal coordinate $s$ is rather weak, and the last term in the latter formula for $w$ is negligible, especially in central parts of large ice sheets where $A \to 0$.

In the framework of the shallow-ice approximation [8, 9], heating is due to the plastic (shear) deformations in the glacier body and takes the form [3]:

$$Q = g\rho(1-\zeta)\left|\frac{\partial l}{\partial s}\right|\left|\frac{\partial u}{\partial \zeta}\right| \tag{6}$$

and is fully determined by Eqs. 5.

Accordingly, the particle derivative of temperature $T$, in parentheses on the left-hand side of Eq. 1, can be expressed in terms of variables $t$, $s$, and $\zeta$ [2]:

$$\frac{dT}{dt} \equiv \frac{\partial T}{\partial t} + u\frac{\partial T}{\partial s} + w\frac{\partial T}{\partial z} = \frac{\partial T}{\partial t} + u\frac{\partial T}{\partial s} + \frac{\overline{w}}{\Delta}\frac{\partial T}{\partial \zeta}, \quad (7)$$

where $\overline{w}$ is the effective rate of the ice-mass transfer in the vertical direction.

By definition [2], using Eqs. 3 and 5, we have

$$\overline{w} = \Delta\frac{d\zeta}{dt} = \overline{\rho w} + (1-\zeta)\left(\frac{\partial \Delta}{\partial t} + u\frac{\partial \Delta}{\partial s}\right) - \overline{\rho}\left(\frac{\partial l}{\partial t} + u\frac{\partial l}{\partial s}\right)$$

$$= -b + (1-\zeta)\left[b - w_0 + \sigma\left(b - w_0 - \frac{\partial \Delta}{\partial t}\right)\left(\frac{1-F}{1-\zeta} - 1\right)\right]. \quad (8)$$

It should be emphasized that the introduction of the normalized variable $\zeta$ and the appropriate determination of the vertical ice-mass transfer in accordance with Eqs. 7, 8 automatically take into account both temporal and lateral variations of the ice-sheet thickness and corresponding effects of the longitudinal advection and the snow-firn-ice compressibility on the heat transfer process. The term of the horizontal heat convection on the right-hand side of equality (7) is now responsible only for the impact of boundary (surface and bottom) temperature variations along the ice-flow line on the temperature field in the ice sheet. As a rule, it can be neglected in central areas of ice sheets with small geographical temperature gradients and bottom temperatures close to the ice melting point.

### 2.3. Boundary conditions

To complete the above heat transfer model, we have to set boundary conditions at the bottom and on the free (upper) surface of the ice sheet. The general heat balance equation [3, 9] at the ice-sheet bottom can be used to describe the thermal interaction of the glacier with the underlying substrata:

$$-\frac{\lambda}{\Delta}\frac{\partial T}{\partial \zeta}\Big|_{\zeta=0} = q_0 - \rho_0 L_f w_0 + g\rho_0\Delta\left|\frac{\partial l}{\partial s}\right| u_0 \Big|.$$

Here $q_0$ is the geothermal flux, and $L_f$ is the latent heat of ice fusion. The last term on the right-hand side of this equation is the frictional heating due to the ice sliding over the bedrock. It is zero in the case of a floating ice sheet ($\sigma = 0$ and $\partial l/\partial s = 0$) or when the ice is frozen to the bed ($\sigma = 1$ and $u_0 = 0$).

If the basal layer is below the ice melting point then long-term climatic temperature fluctuations, which penetrate through the ice-sheet thickness can perturb the thermal state of the underlying rocks [14]. This, for example, is the case in central Greenland [15] and at Dome Fuji [16] in Antarctica. Thus the conjugate boundary value problem should be formulated to describe the rock-ice thermal interaction.

However, in Vostok region in central Antarctica, preliminary simulations [1, 17] suggested that the bottom ice was at the fusion temperature $T_f$. Furthermore, direct field observations [18] definitely confirmed the existence of the vast subglacial water reservoir (Lake Vostok). In this particular case, based on the above general equation, we have:

$$T_{|\zeta=0} = T_f\ ;\quad -\frac{\lambda}{\Delta}\frac{\partial T}{\partial \zeta}|_{\zeta=0} = q_0 - \rho_0 L_f w_0\ . \quad (9)$$

Equilibrium pressure-melting temperature $T_f$ at the ice-water interface depends on salinity and on the amount of air dissolved in the water. For the Vostok lake conditions it could vary from –2.5°C, for fresh (pure) water [18], to –3.2°C for air-saturated (or saline) water [19]. As discussed below (section 4), the latter uncertainty might result in different estimates of the ice-sheet thickness constrained from the observed temperature profile at Vostok.

The boundary condition on the free surface of the ice sheet should merely be a given surface temperature $T_s$ as a function of time. However, the upper heterogeneous layer of snow, firn, and bubbly ice deposits, where density $\rho$ and relative thermal conductivity $\Lambda$ in Eq. 1 change rapidly, is rather thin. Its thickness at Vostok is not more than 200–250 m [10, 12], that is about 0.05 in $\zeta$-scale variation. Hence, it would be very convenient for numerical simulations to reduce Eq. 1 to a simpler form, assuming $\overline{\rho} = 1$ and $\Lambda = 1$ in Eqs. 2. To do this without violating the heat balance of the glacier, one has to impose a special boundary condition on the free surface. It is shown by Salamatin et al. [3] that the equation that maintains the same heat flux near the surface and does not change the temperature distribution in the deeper ice layers is

$$-\left[\int_0^1\left(\frac{1}{\overline{\rho\Lambda}}-1\right)d\zeta\right]\frac{\partial T}{\partial \zeta}|_{\zeta=1} = T_{|\zeta=1} - T_s\ . \quad (10)$$

The integral in square brackets can be evaluated explicitly [4] for $\overline{\rho}$ and $\Lambda$ given in Table 1. It accounts for the enhanced thermal resistance of the near-surface glacier strata.

### 2.4. Parametric heat and ice-mass transfer model at Vostok

Eqs. 1–10 yield a parametric heat and mass transfer model for temperature field evolution in central Antarctica, in the vicinities of Vostok Station.

First, we should note [7] that the ice freely floating on the lake surface does not undergo shear deformations, but, in accordance with new seismic data [20], the ice sheet is substantially grounded several kilometers downstream from Vostok so that the bedrock relief may interfere with the basal ice movement. A scheme of the ice flow in the Vostok region is shown in Fig. 1. Preliminary ice-core studies [21, 22] reveal that the maximal shear most probably occurs at intermediate depths (3460–3540 m), overlying the immovable bottom ice. If $z_b$ (or $\zeta_b = (z_b - z_0)/\Delta$) is the lower level of the basal shear then the local ice-flow scheme can approximately be obtained from Eqs. 5 as $\mu \to \infty$ within the interval $0 < \zeta < \zeta_b$.

Further, following Lliboutry [23] and Ritz [17, 24], we represent the exponential function $\mu(T)$ for $\zeta > \zeta_b$ as the power relation

$$\mu(T) \approx \mu_b\left(\frac{1-\zeta}{1-\zeta_b}\right)^{\alpha-\beta}\ ,\quad \beta > \alpha\ , \quad (11)$$

where $\mu_b$ is the viscosity factor in the basal shear layer. The apparent ice-flow exponent $\beta$, estimated by Lliboutry, adjusts ice rheology to non-isothermal conditions (to the temperature gradient in the ice-sheet thickness) and is considered hereinafter as a tuning parameter (see Table 1).

The substitution of Eq. 11 into Eqs. 5 reduces the integrals to explicit expressions and yields

$$\left|\frac{\partial l}{\partial s}\right| = \frac{1}{g\rho_0\Delta}\left[\frac{\sigma\mu_b(\beta+2)|A|}{\Delta^2(1-\zeta_b)^{\alpha+2}}\right]^{\frac{1}{\alpha}};$$

$$G(\zeta) = \frac{\beta+2}{\beta+1}\left[\frac{(1-\zeta_b)^{\beta+1}-(1-\zeta)^{\beta+1}}{(1-\zeta_b)^{\beta+2}}\right], \quad (12)$$

$$F(\zeta) = 1-(1-\zeta)G(\zeta)-\left(\frac{1-\zeta}{1-\zeta_b}\right)^{\beta+2}, \quad \zeta \geq \zeta_b.$$

Both functions $G$ and $F$ are equal to zero when $0 \leq \zeta < \zeta_b$.

Finally, Eqs. 1, 2, 6–10, with the use of Eqs. 12, can be transformed to the quasi-one-dimensional heat-transfer model, which generalizes previous results [3, 4].

$$\rho_0 c\Delta^2\left(\frac{\partial T}{\partial t}+\frac{\overline{w}}{\Delta}\frac{\partial T}{\partial \zeta}\right) = \frac{\partial}{\partial \zeta}\left(\lambda\frac{\partial T}{\partial \zeta}\right)+\overline{Q},$$

$$-t_0 < t < 0, \quad 0 < \zeta < 1; \quad (13)$$

a) $T_{|t=-t_0} = T_0$; b) $T_{|\zeta=0} = T_f$;

c) $$-\frac{\chi}{\Delta}\frac{\partial T}{\partial \zeta}|_{\zeta=1} = T_{|\zeta=1} - T_s;$$

$$\overline{Q} = \begin{cases} 0, & 0 \leq \zeta < \zeta_b \\ g\rho_0\Delta\left|\frac{\partial l}{\partial s}\right|\frac{\sigma(\beta+2)|A|}{(1-\zeta_b)^{\beta+2}}(1-\zeta)^{\beta+1}, & \zeta \geq \zeta_b \end{cases}$$

$$\overline{w} = \begin{cases} -w_0 - \zeta\left[(1-\sigma)(b-w_0)-\sigma\frac{\partial\Delta}{\partial t}\right], & 0 \leq \zeta < \zeta_b \\ -b+(1-\zeta)\left[b-w_0+\frac{\sigma}{(\beta+1)(1-\zeta_b)}\left(b-w_0-\frac{\partial\Delta}{\partial t}\right)\left(1+\zeta_b(\beta+1)-\left(\frac{1-\zeta}{1-\zeta_b}\right)^{\beta+1}\right)\right], & \zeta \geq \zeta_b \end{cases}$$

$$w_0 = \left(q_0 + \frac{\lambda}{\Delta}\frac{\partial T}{\partial \zeta}|_{\zeta=0}\right)\Big/\rho_0 L_f.$$

The initial thermal state of the glacier $T_0$ is assumed at a certain time $t_0$ (BP) far in the past; $\chi$ is the apparent heat transfer coefficient at the glacier surface, defined by Eq. 10 and given in Table 1.

It should be noted that the spatially quasi-one-dimensional formulation of model (13) becomes possible due to the special normalization of the vertical coordinate $\zeta$ and appropriate determination of the vertical ice-mass transfer rate $\overline{w}$. The corresponding horizontal component of the heat convection in Eq. 7 was estimated in [3] as negligible. C. Ritz (personal communication) confirmed by numerical tests the validity of such approximation for the Antarctic Plateau, with its small geographical temperature gradients.

In fact, the above boundary value problem, relating the mass-balance and surface-temperature histories at a certain site on the ice sheet surface to the temperature evolution in the glacier depths, is not absolutely local and complete. One of its principal parameters, ice-equivalent thickness $\Delta$, is a result of the global ice-sheet dynamics also influenced by past climate changes. Thus, a supplementary model should be developed to provide a consistent parametric presentation of the climatic input $b$, $\Delta$, and $T_s$.

### 2.5. Climatic submodel

In accordance with Robin [25], precipitation in Antarctica can be correlated to the water-vapor equilibrium pressure in the atmosphere at the top of the inversion layer and, consequently, to the condensation (inversion) temperature $T_i$ in clouds.

Certainly, the geographical distribution of accumulation rate is not uniquely governed by the local inversion temperatures and precipitation. In addition to snowfall, it depends on atmospheric circulation and wind scour, especially in cold central regions where the precipitation itself is very low. However, the saturation vapor pressure and the inversion temperature represent the right tendency of temporal changes in the accumulation rate. Thus, the past values $b$ can be, at least approximately, calculated as today's local value $b^0$ (found at Vostok Station in [26]) corrected by the exponential factor, which is the function of the inversion temperature fluctuations $\delta T_i$ counted from its contemporary level $T_i^0$. The corresponding computational procedure was elaborated and described by Ritz [17, 24]:

$$b = b^0 \exp(\eta_b \delta T_i), \tag{14}$$

where $\eta_b$ is the factor which accounts for all the precipitation mechanisms. In accordance with Ritz's estimations for the Antarctic Plateau, this parameter is mainly determined by the dependence of water–vapor saturation pressure in air on temperature which is given by Magnus's empirical formula (see Table 1).

As it has already been mentioned, the variations of surface elevation in the interior of the ice sheet represent the global response of the whole glacier to the changing climate and are not local by their nature. Special investigations conducted by Salamatin and Ritz [5] revealed two major mechanisms that control this process. They are: (1) the hydrodynamic interaction between a time-lagging low-accumulation-rate interior of a large ice sheet and its active high-accumulation-rate coastal zone and (2) the feedback between the inland surface elevation and its growth linked through the ice-flow rate. As a result, the evolution of the ice-equivalent thickness $\Delta$ in the central area of the ice sheet is described by a nonlinear ordinary differential equation which can be written

$$\frac{\partial \Delta}{\partial t} = (1 + e_b)\left[b - sign\Psi |\Psi|^{\alpha} \langle b \rangle\right], \tag{15}$$

$$\Psi = 1 - \gamma_b \left[ \left( \frac{b}{\langle b \rangle} \right)^{\frac{1}{\alpha}} - 1 \right] + \gamma_l \left[ \left( \frac{\Delta}{\langle \Delta \rangle} \right)^{\frac{2\alpha+2}{\alpha}} - 1 \right].$$

Hereinafter the angle brackets $\langle \cdot \rangle$ denote the constant component of a characteristic, i.e. its value averaged over the periods of climatic cycles; $e_b$ is the relative excess of the mean accumulation rate in the central region of the ice sheet over the local accumulation rate $b$ at the site (Vostok) under consideration.

The two coefficients $\gamma_b$ and $\gamma_l$ in Eq. 15 are the principal tuning parameters attributable to the global behavior of the glacier. They have a clear physical meaning. The first one introduces the effect of practically instantaneous adjustment of the margins to changes in mass balance. This accordingly dams or unlocks the ice-mass transport from the central part of the ice sheet and amplifies the fluctuations of its surface elevation. The second one represents the feed-back which counterbalances changes in accumulation rate and ice-sheet thickness (ice flow). Parameters $\gamma_b$ and $\gamma_l$ have complex structure [5] and depend on a large number of glacier characteristics and existence conditions. Their values (Table 1) were estimated and verified in [5] for the Vostok region through the intercomparison with hydrodynamic predictions of general

model [24]. Eq. 15 is now included in our model [6, 7] instead of its high-frequency approximation ($\gamma_b$, $\gamma_l = 0$) used earlier by Ritz [17] and Salamatin et al. [3, 4]. The initial ice-sheet thickness $\Delta(t = -t_0)$ is chosen so as to reach the present-day value $\Delta(t = 0) = \Delta^0$.

It is also worth noting that, in accordance with similarity theory and scale analysis [27–29] of the general equations governing ice-sheet dynamics, the typical basal viscosity factor $\mu_b$ in Eqs. 11, 12 is closely related [5] to the dimensionless number $K_l$ which is the ratio between the global vertical scale (average thickness) of the ice sheet and its thickness at the site of the study. For the present-day conditions,

$$K_l = \left[\frac{\mu_b b^0 (1+e_b)}{(g\rho_0)^\alpha s_0^{\alpha+1}}\right]^{\frac{1}{2\alpha+2}} \frac{s_0}{\Delta^0},$$

where $s_0$ is the length of the reference flow line.

Consequently, for the local ice-sheet surface slope and ice flow rate instead of Eqs. 4, 12 we can write

$$\left|\frac{\partial l}{\partial s}\right| = \frac{\Delta}{s_0}\left[\frac{\sigma(\beta+2)|A|}{s_0 b^0 (1+e_b)(1-\zeta_b)^{\alpha+2}}\left(\frac{K_l \Delta^0}{\Delta}\right)^{2\alpha+2}\right]^{\frac{1}{\alpha}},$$

$$|A| = \bar{s}_d s_0 (1+e_b)\langle b\rangle |\Psi|^\alpha . \qquad (16)$$

Here $\bar{s}_d$ is the reduced distance from the ice divide (ridge $B$) normalized by $s_0$ and defined as an apparent quantity which takes into account the divergence of the flow lines. It can easily be seen from Eqs. 16 that the model equations (13)–(15) do not depend explicitly on the length of the flow line $s_0$. Parameters $K_l$, $\bar{s}_d$, and $e_b$ can be estimated (see Table 1) directly from the available geographical data [5, 30, 31].

### 2.6. Summary of the modeling approach

Thus, for any surface temperature $T_s(t)$ and related inversion-temperature variations $\delta T_i(t)$, as functions of time $t$, the temperature distribution $T(z, t)$, the accumulation rate $b(t)$, and the ice-sheet thickness $\Delta(t)$ are determined by Eqs. 13–16, provided that the model parameters in Table 1 are set up and tuned to the environmental conditions. Based on the shallow-ice approximation and the flow line theory, the spatially one-dimensional formulation of the model is simplified for conditions in the central parts of large ice sheets, in particular for Vostok region in Antarctica. Snow-firn-bubbly ice compressibility effects and subglacial lake existence are taken into account. Most of the uncertainties in the general mathematical description and the input data are presented through this approach in the parametric form without significant loss of the model generality itself. The tuning parameters have clear physical meaning.

A special interactive computer system was developed on the basis of the constructed model. It is aimed at ice-core dating and paleoclimatic reconstructions with the use of borehole temperature-depth profiles and isotopic records. The further sections of this paper actually follow the items of the main menu of this system.

At the end of the model presentation, it is important to point to the principal assumption underlying the above mathematical considerations and restricting their validity. That is the time invariant spatial patterns of accumulation rate and ice-sheet flow which only make the fixed-flow-line theory acceptable. This may originally cause an additional uncertainty in the vertical

velocities that could manifest itself first of all through the temporal change in the model parameters $\sigma$, $\bar{s}_d$, $e_b$, and to a lesser degree in $\eta_b$. This question was discussed in [4, 6] and is considered below in connection with the general problem of parametric sensitivity of model predictions and inversion procedures.

## 3. Borehole temperature memory

### 3.1. First-guess estimates

To understand the nature of the paleotemperature records preserved as transient temperature fields in ice-sheet thickness, let us consider a basic process of thermal-wave propagation in a homogeneous ice-filled semi-space along the $h$-axis, which is directed downward perpendicular to the boundary plane (Fig. 2). The ice moves at constant velocity $v$ in the $h$-direction and is specified by constant thermal diffusivity $k = \lambda/(c\rho)$.

Cosine harmonic temperature oscillations of a unit amplitude with frequency $\omega$ (period $2\pi/\omega$) on the semi-space surface induce (see Fig. 2) a spatial thermal wave $T$ of the same time period propagating along the $h$-axis with phase lag $\psi$ and exponentially damped amplitude $A$ [32]

$$T(h,t) = A\cos(\omega t - \psi); \qquad (17)$$

$$A = \exp\left\{-h\sqrt{\frac{\omega}{2k}}\left[\left(\sqrt{1+\varepsilon^2}+\varepsilon\right)^{\frac{1}{2}} - \sqrt{2\varepsilon}\right]\right\},$$

$$\psi = h\sqrt{\frac{\omega}{2k}}\left(\sqrt{1+\varepsilon^2}-\varepsilon\right)^{\frac{1}{2}}, \qquad \varepsilon = \frac{v^2}{4k\omega}$$

Eq. 17 shows that the most recent peak (or trough) in the surface-temperature variations which occurred at the moment $t_* = -\pi/\omega$ in the past can be distinguished at the present time with the amplitude $A_*$ at depth $h_*$, where the phase lag $\psi(h_*) = \pi$. Previous fluctuations would be represented by much smaller anomalies with amplitudes of the order of $A_*^2$, $A_*^3$,... at depths $2h_*$, $3h_*$,..., respectively. In most cases they are vanishingly small. Thus, the general limitation of the borehole temperature memory is that this older part of the surface-temperature history is erased and cannot be distinguished in the ice.

We estimate $v = 2.4$ cm·yr$^{-1}$ in central Antarctica (Vostok [26]) and $v = 25$ cm·yr$^{-1}$ in central Greenland [33]; thermal diffusivity is $k = 1.8\cdot10^{-6}$ and $1.3\cdot10^{-6}$ m$^2$·s$^{-1}$, respectively, after [32]. The rounded characteristics $h_*$ and $A_*$ of the remembered signal for different time scales (periods) of the surface-temperature perturbations are given in Table 2. Although rather rough, these calculations explicitly reveal the principal peculiarities of the temperature memory and, among them, its essential sensitivity to the environmental conditions, such as the rate of ice accumulation and the ice thickness.

The main result is that both thermal diffusion and advection within an ice sheet of finite thickness work as a "window" filter with respect to the original climatic signal. The high-frequency fluctuations of the surface temperature, those with time scales less than 1 kyr and comparatively small amplitudes (~1°C), are almost completely filtered out in the upper part of the ice sheet (above a depth of 200–300 m). The level of the "noise" induced in the deeper strata has the order of 0.01–0.05°C. On the other hand, the long-term temperature variations do not produce a detectable wave-shape record in the vertical temperature profile

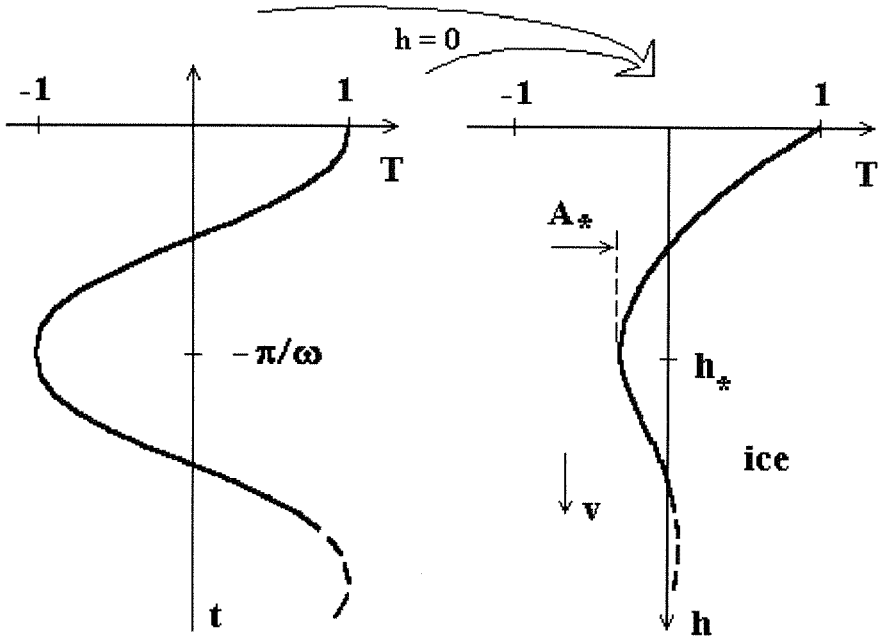


Figure 2: The thermal-wave propagation induced in moving ice by the cosine temperature fluctuations on the ice surface ($h = 0$). The most recent peak (or trough) in the surface-temperature variations can be distinguished at the present time with the amplitude $A_*$ at depth $h_*$.

which follows the slow changes in the surface temperature, remaining quasi-stationary because of insufficient thickness of the ice. As can easily be seen from Table 2, the low-frequency threshold is significantly affected by the vertical velocity of the ice. From this point of view, the low-accumulation areas of central Antarctica, in the vicinities of Vostok Station with the ice thickness exceeding 4000 meter, are the unique regions on the Earth. The frequency band of the deep borehole temperature record here covers the widest range of periods up to 100 kyr, including all the main climatic (astronomic) cycles [34]. For past (Pleistocene) temperature variations of about 10–15°C the expected anomalies in the thermal state of the glacier would be not less than 0.5–1°C (see Table 2). At the same time, the temperature-memory length of the relatively thin (~3000 m) and high-accumulation central part of the Greenland ice sheet is practically limited by the Last Glacial Maximum (LGM), i.e. by the time scales of 20-30 kyr. However, a noticeable difference in the memory resolution should be emphasized. The Greenland ice temperatures still keep from 10 to 60 % of the initial amplitudes of the recent paleo-temperature fluctuations, while the respective level in Antarctica is much lower, not exceeding 5–8 %. This means, for example, that the Holocene (1–10 kyr) climate history with 2–5°C temperature changes is recorded in Greenland (see Table 2) as a temperature-depth wave signal with the amplitudes not less than 0.3–1.5°C, but in Antarctica the same climate periods would be represented only by the ice-

Table 2: Relative amplitude levels and penetration depths of recent surface-temperature fluctuations remembered in central parts of the Antarctic and Greenland ice sheets.

| Time scales of perturbations, yr | Antarctica | | Greenland | |
|---|---|---|---|---|
| | $h_*$, m | $A_*$ | $h_*$, m | $A_*$ |
| 80 | 120 | 0.04 | 100 | 0.06 |
| 310 | 240 | 0.04 | 200 | 0.08 |
| 1250 | 470 | 0.05 | 420 | 0.12 |
| 5000 | 940 | 0.05 | 930 | 0.25 |
| 20000 | 1900 | 0.06 | 2700 | 0.56 |
| 40000 | 2700 | 0.07 | *not traced* | |
| 100000 | 4200 | 0.08 | *not traced* | |

temperature perturbations of the order of 0.1–0.3°C.

Numerous earlier computational simulations [1, 14, 17, 35–38] and special sensitivity tests performed for Vostok conditions in [6] fully confirm the above estimates and go into many additional details of the transient temperature processes in ice sheets, using more elaborate modeling techniques and based on various experimental data. Nevertheless, the simplified approach, we have employed here, is the most obvious way to show that the temperature-depth profiles in ice sheets have a very specific, selective and relatively short, memory. The direct informational value of these paleoclimatic records was theoretically estimated by Rommelaere [39] as rather low. The preserved information non-uniformly represents the past climate. For instance, in the Vostok region 75 % of the informational capacity corresponds to the recent 6-kyr period and only 5 % describe the climate history from 15 to 30 kyr BP.

All these analyses lead us to the principal conclusion that the inverse problem of paleotemperature reconstructions from borehole thermometry should be considered as an essentially ill-posed problem, which does not have, in general, a unique and stable solution.

### 3.2. Regularization and inverse procedures

Now it is easy to realize that there exists an infinite set of significantly different surface-temperature histories resulting in the same present-day temperature-depth profile within the accuracy limits of measurements. Thus, any direct inverse method cannot be applied successfully to infer past temperatures on ice-sheet surface from borehole thermometry unless the inverse procedure itself is combined with a regularization approach. That is we have to restrict our choice of acceptable solutions, basing on our *a priori* knowledge or/and assumptions about the paleoclimate and its transformation in the ice memory. In practice, this suggests an appropriate parametric reduction of the plausible past surface-temperature variations in accordance with what is actually kept by and can be observed in the ice sheet. The latter question is the key one.

A special issue [40] was addressed to the problem of paleoclimatic processing of underground temperature distributions controlled by thermal diffusion in rocks.

In the case of the Greenland ice sheet, where reliably remembered (LGM–Holocene) climate is comparatively short, the straightforward, natural regularization is to damp back through time the searched surface-temperature fluctuations, keeping only longer and longer time-scale trends till the limit of their resolution. To perform such a procedure, one can simply divide the temperature history into a number of intervals which lengths are related to the accuracy of the borehole-temperature measurements and progressively grow in the past. Unknown temperatures, constant within each interval, form the set of parameters to be determined through an inverse procedure. This line of the study was elaborated in [37, 38, 41, 42]. Additional constraints on the surface temperature behavior were also considered [38, 41] to "regularize" the solution of the inverse problem. Different least-square minimization and optimal control methods were applied to fit the borehole temperature data and to infer past climate in Greenland. A very useful discussion [43, 44] revealed how crucial the temperature-history parameterization was in accounting for data uncertainties to avoid over-fitting and to match the actual information provided by the borehole-temperature profile. The probabilistic formulation of the inverse problem and the use of the Monte Carlo method [45, 46] give the most direct and complete presentation of errors and resolution properties of the inferred surface-temperature history [42].

Passing to the interpretation of Antarctic ice-sheet temperatures, we follow the research by Salamatin et al. [3, 4, 6, 7]. One should note that, in accordance with the above preliminary estimates (see Table 2), unlike Greenland, the Holocene climate history does not strongly affect temperature fields in central Antarctica, especially in their deeper part. Only recent long-term surface temperature oscillations with periods from 20 to 100 kyr and relatively high amplitudes can be remembered in the ice-sheet. The principal assumption is made that Milankovich astronomic cycles prevail in the Pleistocene climate changes depicted in the known paleoclimatic marine and ice-core records, e.g. [31, 47–61]. Hence the inverse problem may be formulated primarily to infer the dominant "metronomic" part of local paleotemperature history at Vostok by fitting computed and measured borehole temperature profiles. Accordingly, to constrain the inverse procedure and, thus, to "regularize" its solution, we express the inferable components of the surface temperature oscillations $T_s(t)$ as a sum of harmonics of Milankovich (eccentricity, obliquity, and precession) periods $t_1 = 100$, $t_2 = 41$, and $t_3 = 23$, $t_4 = 19$ kyr:

$$T_s(t) = \langle T_s \rangle + \sum_{i=1}^{4} [A_i \cos(\omega_i t) - B_i \sin(\omega_i t)], \quad -t_0 < t < 0, \qquad (18)$$

where frequencies $\omega_i = 2\pi / t_i$ are fixed and only the amplitudes (and the phase lags) $A_i$, $B_i$ ($i$ = 1,...,4) are to be found; $\langle T_s \rangle$ is the averaged surface temperature.

Hereinafter the value $t_0$ is taken as $t_0 = 5t_1 = 500$ kyr, and the initial thermal state $T_0$ of the glacier at the far moment $t_0$ (BP) in the past in Eq. 13a is defined as a stationary state corresponding to $T_s \equiv \langle T_s \rangle$.

As for the inversion temperature perturbations in Eq. 14, an approximate simplified relation is assumed at this step, after [53, 62]:

$$\delta T_i / \delta T_s = C_i, \qquad \delta T_s = T_s(t) - T_s^0 \qquad (19)$$

with the factor $C_i = 0.67$.

Eq. 19 is thought to represent the right tendency of the $\delta T_i$ variations [63] and is not crucial as far as the general dominant climatic events are concerned. However, it should be emphasized that the response of $T_i$ and $T_s$ to the orbitally induced perturbations may not be identical due to the complex non-linear heat balance at the glacier surface, including thermal radiation and heat exchange with the atmosphere. For instance, the inversion strength $T_i - T_s$ is more likely linked [63, 64] to the difference between July and January surface temperatures. Thus, it could be additionally influenced by the higher precession oscillations of the seasonal temperatures in comparison with the annual temperature variations predicted for central Antarctica by Short et al. [65]. We come back to this discussion below in section 4. Here we would like to stress that $T_s$ is not only distinguished from $T_i$, but is also not assumed to be equal to the surface-air temperature. The variations of the ice-sheet surface temperature ($\delta T_s$) might be not merely proportional to those of the inversion temperature ($\delta T_i$), as Eq. 19 suggests. A more general form of this equation was introduced in [6] and is used in the next section.

Discrepancy between the computed present-day temperature profile $T(z, t = 0)$ and an experimental temperature $T_{ex}(z)$ observed in a deep borehole can be estimated as the mean-square deviation $S$

$$S(A_i, \ldots, B_i, \ldots; \langle T_s \rangle, T_f, q_0, \ldots) = \left\{ \frac{1}{N} \sum_{k=1}^{N} \left[ \frac{T_{ex}(z_k) - T(z_k, t=0)}{\nu_k} \right]^2 \right\}^{\frac{1}{2}}. \qquad (20)$$

Here $z_k$ are the measurements points and $\nu_k$ are the weighting factors proportional to the standard deviations of the measurement errors at these points, $k = 1, \ldots, N$. Thus, the inverse procedure is reduced to minimizing the target norm $S$ as a function of $A_i$, $B_i$ ($i = 1, \ldots, 4$) and, maybe, $\langle T_s \rangle$, $T_f$ and $q_0$, at given values of $\nu_k$, $C_i$, and the other model parameters (see Table 1): $\Delta^0$, $b^0$, $\sigma$,....

It should be recognized that both the initial basic assumption and the above regularization procedure are somewhat limiting. Following general conceptions of Milankovich theory [49, 50], they imply quasi-linear response of Earth's climate to orbital forcing, disregarding "climatic noise", with fixed constant frequencies and phase shifts (supposed to be determined) in the dominant "metronomic" part of local paleotemperature oscillations given by Eqs. 18 and 19. The latter step is an approximation even in the framework of Earth astronomy [34] and is supposed to be valid only within a relatively short interval of cosmic history not exceeding several recent glacial-interglacial cycles. Another peculiarity is linked to the introduction of the 100-kyr-eccentricity period into Eq. 18. This radiation astronomic cycle is thought to be too small in amplitude and rather late in phase to produce the corresponding climate cycle by direct forcing, although there exist various plausible explanations of its even dominant presence in global climate changes, which were reviewed by Imbrie et al. [50]. In any case, the computational tests

conducted and discussed in [6] prove that the cycle is not an artifact, and that such a harmonic with a period $t_1$ at least close to 100 kyr is actually present in the borehole-temperature record. Furthermore, it is clear that, for each of the harmonic components, which can be revealed in the surface temperature variations, the temperature profile mostly reflects their recent periods and that any use of Eq. 18 at greater times is a mere periodic extrapolation. Nevertheless, we still hope that the main climate changes might be predicted and dated [4, 6, 7] by these series and that the set of trigonometric functions in Eq. 18 can be regarded as an appropriate mathematical basis to expand the dominant part of $T_s(t)$.

The formulation of the inverse problem is not complete without experimental borehole temperature data ($T_{ex}$). Since the beginning of the deep drilling program at Vostok Station in 1970, a number of temperature surveys have been performed by specialists from St. Petersburg Mining Institute in different holes. Geophysical studies that were carried out before 1983 to a depth of about 2040 meters were summarized in [12]. Temperature observations were repeated several times during 1983–1988 in borehole 3G [1, 3, 4]. The most accurate data within the upper 1950-meter strata were obtained by Yu. Rydvan in 1988 [4]. The absolute (systematic) error of his measurements was estimated as ±0.05°C, while the reproducibility was found to be 0.005–0.01°C. The first type of error could induce a shift in the experimental temperature profile rather than a false wave-like signal detectable by the inverse procedure. Another temperature profile was measured in 1993 in 2755-meter deep borehole 5G by A. Volkov mainly below the depth of 1950 m six months after the thermal-drilling operations had been stopped. For the latter reason the accuracy of these data was much lower. In the 1996–1997 season the bottom of the mechanically drilled borehole 5G reached a depth of about 3523 m and during the next season, after the ten-months break in drilling, the temperature logging was extended by R. Vostretsov from 1900 m to this extreme level. The absolute error of his gauge did not exceed ±0.07°C, and the sensitivity was not worse than 0.01–0.02°C. At the end of the 1997–1998 season, shortly after the new round of mechanical drilling had been finished at the record depth of 3623 m, the measurements were repeated by J.R. Petit. Here we use the stacked 3600-meter deep temperature-depth curve [7] compiled from the borehole surveys performed at Vostok Station during the recent decade with corrections due to logging cable elongation and hole inclination. Unfortunately, its errors, being distributed with a standard deviation of about 0.01°C in the upper part of the ice sheet, increase by almost one order of magnitude near the bottom, and are estimated to average about 0.04°C [7]. Accordingly, hereinafter, in Eq. 20 we assume $\nu_k = 1, 4, 6$ for Rydvan's, Volkov's, Vostretsov's and Petit's measurements, respectively.

The consistency of different paleoclimatic reconstructions based on the shallow [4, 6] and extended [7] temperature profiles confirms their informational value. Certainly, the use of the more complete set of data is preferable.

The minimization of the target function $S$ is performed sequentially by combining the gradient method of steepest descent with the singular-value-decomposition and Newton methods. The resolution and uncertainty of the inverse problem solution

are estimated by the Monte Carlo method [45, 46].

### 3.3. Milankovich cycles remembered in the Vostok borehole-temperature profile

Here we summarize the previous results [3, 4, 6] and continue our preliminary computational experiments [7] with the deep stacked temperature profile, using more sophisticated ice flow and heat transfer models (13)–(16) and the improved formulation of the inverse problem (Eqs. 18–20) with the weighted mean-square deviation norm $S$. All model input parameters are brought together in Table 1.

As has already been mentioned (section 2), new seismic and ice-core data [20–22] indicate that the basal ice flow in the Vostok region may be dammed by the bedrock rise (see Fig. 1) at the edge of the subglacial lake downstream from Vostok. Thus, in general, two plausible scenarios can be suggested [7]:

I. The upper 3540-meter stratum of the ice sheet overlies the immovable bottom ice and is subjected to intensive shear and strain heating within the contact zone.

II. There is no shear deformations in the freely floating ice, and strain heating in the glacier is negligibly small.

Case I corresponds to $\sigma = 1$ and seems to be more realistic, while case II is modeled at $\sigma = 0$ and should be considered as a limiting situation useful for estimating stability of the inverse problem to the ice flow patterns.

The main results of the metronomic signal reconstructions for the two cases are given in Tables 3 and 4 and are also plotted in Fig. 3 for the variant I.

The revised estimation of the factor $\chi$ in model (13) based on Vostretsov's et al. [12] and Sturm's [13] data (see Table 1) shifted the inferred surface temperatures down by 0.5°C in comparison with [6, 7], and a plausible range of the averaged surface temperature $\langle T_s \rangle$ was taken from −64.0 to −62.8°C.

To estimate the inverse solution uncertainty we employed Monte Carlo method [45, 46], assuming that the mean weighted variance of the temperature measurements was close to their squared deviation from the simulated best-fit temperature profile: $S \approx 0.01$°C. Eleven model parameters $A_i$, $B_i$ ($i = 1,..., 4$), $\langle T_s \rangle$, $T_f$ and $q_0$ were subjected to the resolution analysis at the present-day ice-sheet thickness $h_0$ fixed as 3773 m ($\Delta^0 = 3740$ m in ice equivalent, see Table 1). $1.5 \cdot 10^5$ samples were tested during the random walk at a 30 % level of acceptance by the Monte Carlo scheme. Each 50-th accepted set of parameters for which the misfit function $S$ was less than 0.02°C was selected, and in total about 1000 different surface-temperature histories and bottom conditions were collected.

The mean values of the model parameters and their standard deviations, found through the random walk procedure, are given in Table 3. They also present examples of the best-fit solutions to the inverse problem. For case I, the mean metronomic surface temperature oscillations are depicted in Fig. 3a by curve 1 (thick solid line) and are extrapolated into the future (dotted line). Curves 2 (thin lines) show the standard deviations of the reconstruction. The variance bounds of the simulated present-day temperature profiles are drawn in Fig. 3b by dashed lines. They correspond to $S \approx 0.014$°C and confine more than 80 % of all experimental points (dots) which represent the deviations of the

Table 3: Metronomic signal parameters and conditions at the ice sheet bottom estimated by the random walk procedure in case I (shear deformation in the 3540-m stratum of the ice sheet overlying the immovable ice) and case II (no shear in the freely floating ice).

| Parameter | Case I | | Case II | |
|---|---|---|---|---|
| | Mean | STD | Mean | STD |
| $A_1$, °C | 6.89 | 0.73 | 3.40 | 0.39 |
| $A_2$, °C | 4.75 | 1.11 | 8.30 | 0.76 |
| $A_3$, °C | −4.89 | 0.81 | −4.28 | 0.57 |
| $A_4$, °C | −1.66 | 0.71 | −2.23 | 1.04 |
| $B_1$, °C | −2.61 | 1.41 | −0.52 | 0.98 |
| $B_2$, °C | −1.17 | 1.07 | 0.96 | 1.05 |
| $B_3$, °C | 1.56 | 1.24 | 0.62 | 2.13 |
| $B_4$, °C | −2.89 | 1.14 | −3.34 | 1.72 |
| $\langle T_s \rangle$, °C | −63.51 | 0.34 | −63.63 | 0.26 |
| $T_f$, °C | −2.67 | 0.22 | −2.60 | 0.16 |
| $q_0$, W·m$^{-2}$ | 0.0353 | 0.0087 | 0.0124 | 0.0061 |
| $S$, °C | 0.0095 | | 0.0101 | |

Table 4: Ice-sheet conditions derived from Milankovich signal reconstructions at Vostok Station.

| Characteristics | Case I | | Case II | |
|---|---|---|---|---|
| | Mean | STD | Mean | STD |
| Present-day surface temperature, °C | −58.42 | 0.12 | −58.42 | 0.12 |
| Holocene-optimum surface temperature, °C | −53.2 | 0.9 | −53.0 | 0.9 |
| LGM surface temperature, °C | −77.6 | 3.1 | −80.1 | 2.1 |
| Bottom temperature gradient, °C·m$^{-1}$ | 0.0208 | 0.0007 | 0.0209 | 0.0005 |
| Present-day ice-sheet thickness (at $T_f$ = −2.5°C), m | 3781 | 10 | 3778 | 8 |
| Present-day ice-sheet thickness (at $T_f$ = −3.1°C), m | 3752 | 10 | 3749 | 8 |
| Ice accretion rate, mm·yr$^{-1}$ | 1.2 | 0.2 | 3.5 | 0.1 |

temperature measurements from the mean best-fit temperature-depth curve.

It is important to note that many equally good (acceptable) best-fit solutions exist within the variance limits determined by the Monte Carlo method and, in general, they are not presented uniquely by modal values of coefficients $A_i$, $B_i$ ($i = 1,..., 4$). Actually, several intervals for the averaged surface temperature from a wider range $-65.4 < \langle T_s \rangle < -61.8$°C were additionally tested to confirm this fact. Feasible changes in thermophysical properties of ice stated in [11, 12, 32] were considered as well. Every time the amplitudes of the metronomic Milankovich components in Eq. 18 could be respectively adjusted to arrive at the best-fit approximation of the measured temperatures by a simulated profile. The distribution of deviations followed the pattern displayed in Fig. 3b. Table 3 also shows that these parameters may vary considerably, especially between different variants. In spite of this, the principal result [4, 6] remains the same: the total sum of the inferable surface temperature variations, given by Eq. 18, is strongly constrained by the borehole temperature memory, and the major climatic events (peaks and troughs) and their ages are always reliably reproducible. Fig. 3a is a good illustration of the latter conclusion. Thermal conditions at the ice-water interface are also well determined and are close to their modal values in each case (see Table 3).

However, partly due to relatively low accuracy of the deeper part of the stacked experimental temperature profile and partly due to more diverse computational runs in comparison with [4, 6], the variance in ages of single peaks and troughs in metronomic signals is estimated to be about 2.1 kyr on average. That is higher than the value of 1.5 kyr found in [6]. More details concerning the age uncertainty of the climatic events were discussed in [4, 6] and are presented further in section 4 where the Vostok ice core chronology is developed.

Two peculiarities are revealed in computational tests performed with the newly extended borehole temperature observations. First, the geothermal flux from the subglacial lake at the ice-sheet bottom in the vicinities of Vostok Station is found to be noticeably lower than $q_0 \approx 0.053$ W·m$^{-2}$ deduced in [6] and the general prediction of $q_0 \approx 0.054$ W·m$^{-2}$ obtained in [66] for the central part of the Antarctic ice sheet from analysis of the thermal regime above subglacial lakes at more than 50 locations. The reason for this might be that the upper part of the borehole temperature profile, used in [4, 6], represents mainly the general temperature picture typical for the vast central Antarctic region and does not contain sufficient information to distinguish specific local perturbations in the deeper part of the temperature field at Vostok. In both cases I and II the subglacial water freezes at the ice sheet bottom (see Table 4). The latter prediction is in a good agreement with preliminary ice core studies [21, 22] which show that the bottom ice stratum at Vostok, below a depth of 3540 m, is comprised of accreted ice. The rate of accretion varies, being influenced by the 100-kyr-eccentricity cycle in paleoclimatic temperature fluctuations which penetrate through the ice thickness.

Secondly, the metronomic surface temperature variations (Fig. 3a) inferred from the stacked experimental temperature-depth curve are somewhat larger than those deduced earlier from the shallow part in [4, 6]. As before, in all series of computations the present-day temperature

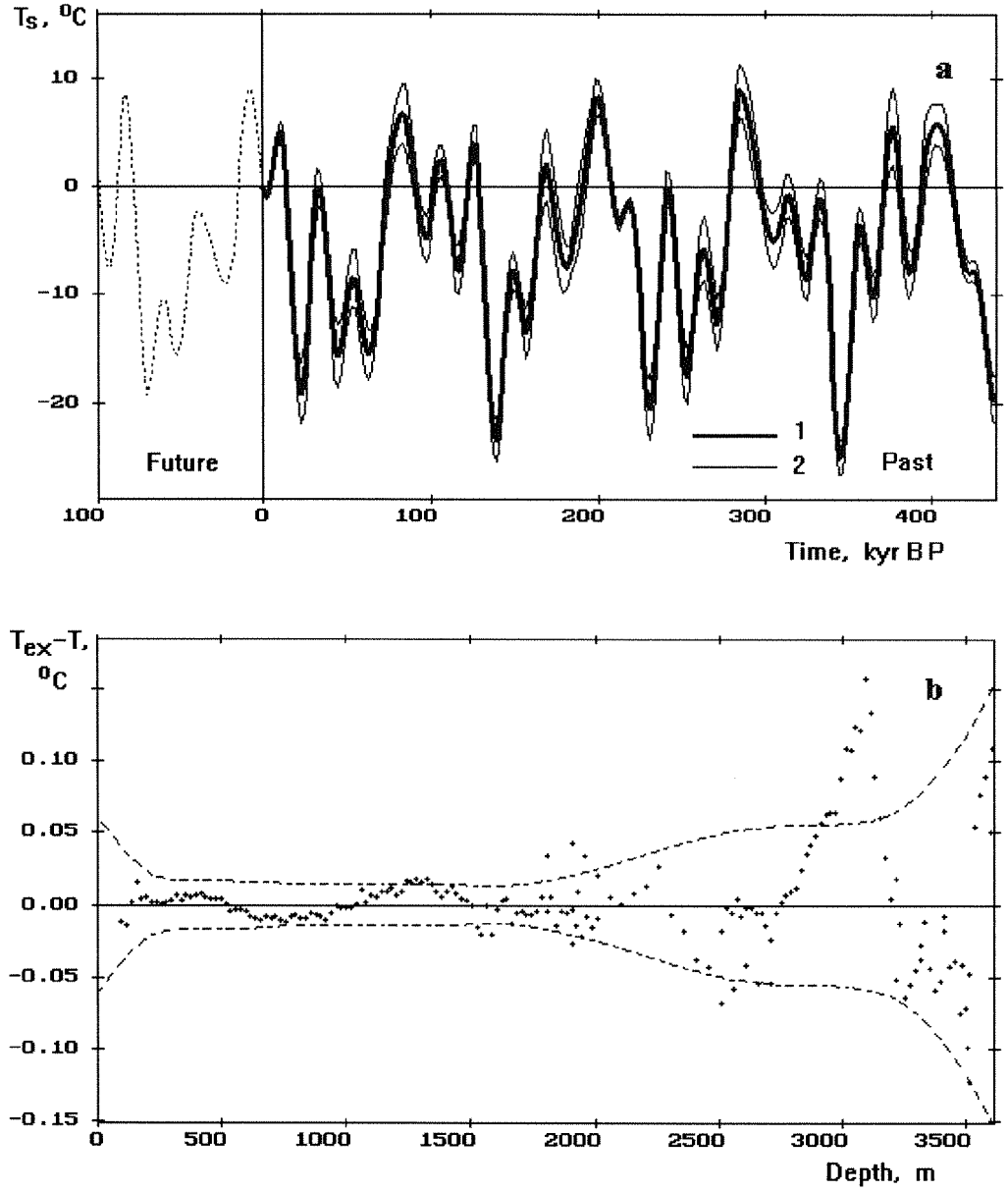


Figure 3: (**a**) Metronomic signal in the Vostok surface temperature variations (curve 1) inferred from the stacked borehole temperature profile and extrapolated into the future (dotted line) in the case I with the shear deformation and strain heating in the 3540-meter stratum of the ice sheet overlying the immovable ice. Curves 2 show the standard deviations of the reconstruction estimated by Monte Carlo sampling. (**b**) Mismatch between the observed and computed (best-fit) temperature profiles within the ice-sheet thickness (dots). The dashed curves are the standard deviation bounds of the simulations which correspond to the target norm $S \approx 0.014$°C.

on the surface of the ice sheet is identically found to be $T_s^0 = -58.42°C$. The standard deviation does not exceed 0.12°C, and this value is hereinafter considered as a reference temperature. It is given in Table 4 together with other data derived in this study in the course of the metronomic signal reconstructions. The difference between the present-day temperature on the ice-sheet surface and meteorological observations of the annual surface-air temperature, –55.5°C at Vostok [26, 53], is quite obvious. The Holocene climatic optimum is also well reproduced as –53.2±0.9°C. The Last Glacial Maximum temperatures in case I (see Fig. 3a and Table 4) are found to be –77.6±3.1°C. They are even lower in case II (see Table 4). Certainly, Eq. 18, being rather flexible in long-term scales, does not describe the details of the recent Holocene–LGM climate period which might be remembered by the borehole temperature. Thus, every time the resulting best-fit metronomes are overtuned by the experimental observations themselves - not only by their errors. Furthermore, the past precession cycles have faded from the borehole temperature memory, and the amount of belief in their high swings revealed in the inferred surface temperature histories should be reduced to minimum. For this reason, paleotemperature reconstructions performed in the next section and based on isotopic ice-core records (direct temperature proxies) are thought to be more accurate. In section 4 it is shown that they result in more moderate estimates of the LGM temperatures than those given in Table 4.

Finally, we would like to emphasize that the present-day thickness of ice at Vostok is not known precisely. Its value is directly related to the ice melting point $T_f$ at the ice-water interface. The simulated borehole temperature profile is practically linear in its bottom part. Hence, the thickness of the ice sheet $h_0 = 3773$ m assumed in our computations can easily be recalculated for any small correction of $T_f$. The bottom temperature gradients and the estimates of $h_0$ determined for pure fresh ($T_f = -2.5°C$) and air-saturated or saline ($T_f = -3.1°C$) water in the subglacial lake are presented in Table 4. The latter estimate is rather close to the recent seismic measurements [20] which estimate a depth at Vostok as $h_0 \approx 3750$ m.

### 3.4. Summary of borehole thermometry analysis

New estimates and computational experiments confirm the general results of earlier studies. Borehole temperature memory in ice sheets has a very specific nature. For each component of the past surface temperature oscillations at a certain time scale only its recent fluctuation (period) can be distinguished in the transient present-day temperature field in the glacier. The memory resolution proportionally fades back through time. Vertical advection and finite thickness of the ice determine its low-frequency limit. Thus, any inverse procedure for paleotemperature reconstructions must be based on an appropriate regularization approach: a reduced (simplified) parameterization of the surface temperature history consistent with informational capacity of the temperature profile and our *a priori* knowledge about past climate features.

From this point of view, central Antarctica (Vostok region) is a unique place where borehole thermometry of the ice sheet may be sufficient to constrain the dominant metronomic part of the past surface

temperature variations presented by the main Milankovich climatic cycles. A random walk Monte Carlo method is employed to solve the inverse problem and to infer the best-fit metronome from the stacked experimental temperature-depth curve at Vostok. Although less accurate, the new deeper part of the profile reveals larger glacial-interglacial temperature fluctuations and lower values of the geothermal flux from the subglacial lake than were estimated before. Ice accretion is now predicted at the ice-water interface (see Table 4). The principal result of the reconstruction remains unchanged. The major climatic events in inferred paleotemperature variations on the ice sheet surface and their ages are reliably reproducible and can be used as time markers to determine chronostratigraphy of isotopic ice-core records. Every time the metronomic Milankovich signals are extended to the maximal age of the ice cores at the bottom of the borehole. The crucial difference between the recent part of the inferred surface temperature oscillations remembered by the borehole temperature profile and their older part which is constrained by the assumption about the Milankovich periodicity determining the climate should be emphasized.

As a general comment, it may be important to mention that one could compare the inferred Milankovich components of the climate response at Vostok (see Table 3) with the original orbital insolation cycles. This might be done as an independent study and needs an expert in this area.

## 4. Ice core age dating and isotropic paleothermometer calibration

### 4.1. Vostok ice core chronology

The ice-core chronology is traditionally obtained by direct modeling of ice sheet dynamics and by computation of ice-flow lines [24, 31, 52, 59, 67]. The problem is that uncertainty of the extended glaciological timescale (EGT) suggested for Vostok ice cores [31] reached, for instance, ±20 kyr mainly due to lack of knowledge about accumulation rate distribution and about basal ice flow conditions upstream of Vostok [24]. Further corrections [56, 59] constrain the chronology to several marine stages discovered in the ice core paleoclimatic records and take into account the existence of the subglacial lake. The estimated accuracy of the refined and further extended glaciological timescale (GT4) is about ±15 kyr. Visual stratigraphic dating [68] and multiparameter continuous count approach [69], recently developed for Greenland ice cores, are thought to have a limited application in central Antarctica because of its extremely low accumulation rates.

Another way of ice age dating is to establish a common temporal framework on the basis of SPECMAP chronology [47, 48, 51] by correlating ice-core climate records with corresponding time series from ocean sediments, e.g. [55, 70–73]. The latter is an important step toward a comparison of glaciological and oceanic paleoclimate archives, although, in this case, besides the inherited errors of the tuning procedures, ±2.5–3.5 kyr [48], we fall into uncertainties which arise from comparing signals of different origins. Additional errors may also be encountered if the age of air bubbles trapped in polar ice is involved [73–75]. The

total accuracy is expected to be not better than ±5–6 kyr. Direct tuning of the Vostok deuterium record to insolation "metronomes" attempted in [55] seems to be more efficient and is thought to be at the accuracy limit of tuning approaches because of the nonlinear climatic response to orbital forcing (climatic noise), estimated as ±4 kyr [49].

The borehole temperature analysis performed in section 3 gives us a new basis for constraining the Vostok ice core timescale. It has been shown that the main climatic cycles and corresponding major events in past surface temperature variations can be restored and their ages are reliably predictable. Once the geophysical metronome is established, the next step is to correlate it with the isotopic temperature record to deduce the ice core chronology [4, 6]. This method automatically takes into account time-averaged constant phase differences between oscillations of Earth's orbital elements and Milankovich cycles in local paleotemperature response. Although it does not eliminate the general errors of tuning approaches, it presents an alternative, independent way for ice-core dating.

The deuterium content ($\delta D$) of the Vostok ice cores from the deep boreholes 3G (2083 m) and 4G (2546 m) was studied in [31, 52, 53]. Isotopic data [56] from the 2755-meter deep 5G core used in [6] have recently been extended to a depth of 3350 m [58, 59]. The stacked continuous deuterium-depth profile [59], which we utilize here for ice core dating and paleoclimatic reconstructions, is plotted by dots in Fig. 4a.

The conventional empirical equation

$$\delta T_i = \left(\delta D - 8\delta^{18}O_{sw}\right)/C_T , \qquad (21)$$

supported by modeling [25, 62, 76], relates deuterium ratios $\delta D$, corrected for changes in the oxygen-isotope composition of ocean water $\delta^{18}O_{sw}$ [48, 51, 73], to inversion temperature fluctuations. $C_T$ is the isotope-temperature temporal slope estimated in [31, 53] for Antarctica as 9 per mil·°C$^{-1}$ from contemporary spatial distributions of isotopes and temperatures.

It is important to note that to actually compare the metronome with the isotopic temperature record and to deduce the ice core timescale, we do not need to know the magnitude of the coefficient $C_T$ in Eq. 21. We have only to assume that the surface and inversion temperatures underwent main climatic changes synchronously, and therefore the smoothed isotopic temperature record is supposed [6] to mimic the inferred metronomic signal.

To filter out high-frequency components a mean square parabolic-spline approximation is applied to the isotope record $\delta D$. The resulting curve is shown by the thin solid line in Fig. 4a. Possible errors in positioning maximums and minimums on the smoothed paleoclimatic signal $\delta D - 8\delta^{18}O_{sw}$ were discussed in [6]. They do not exceed ±10–15 m in the upper half of the record and decrease to ±2–3 m in its deepest part. This makes not more than 0.8–1.0 kyr in age and should be added to the dating uncertainties. The mean ages and depths of the respective peaks and troughs identified in the metronomic surface temperature signal (case I, Fig. 3a) and in the isotope-depth curve (Fig. 4a) are given in Table 5 together with the total correlation errors which take into account all sensitivity tests performed in both cases I and II. The distribution of errors clearly reveals the alternating regions with high and low uncertainty of the age dating procedure. The

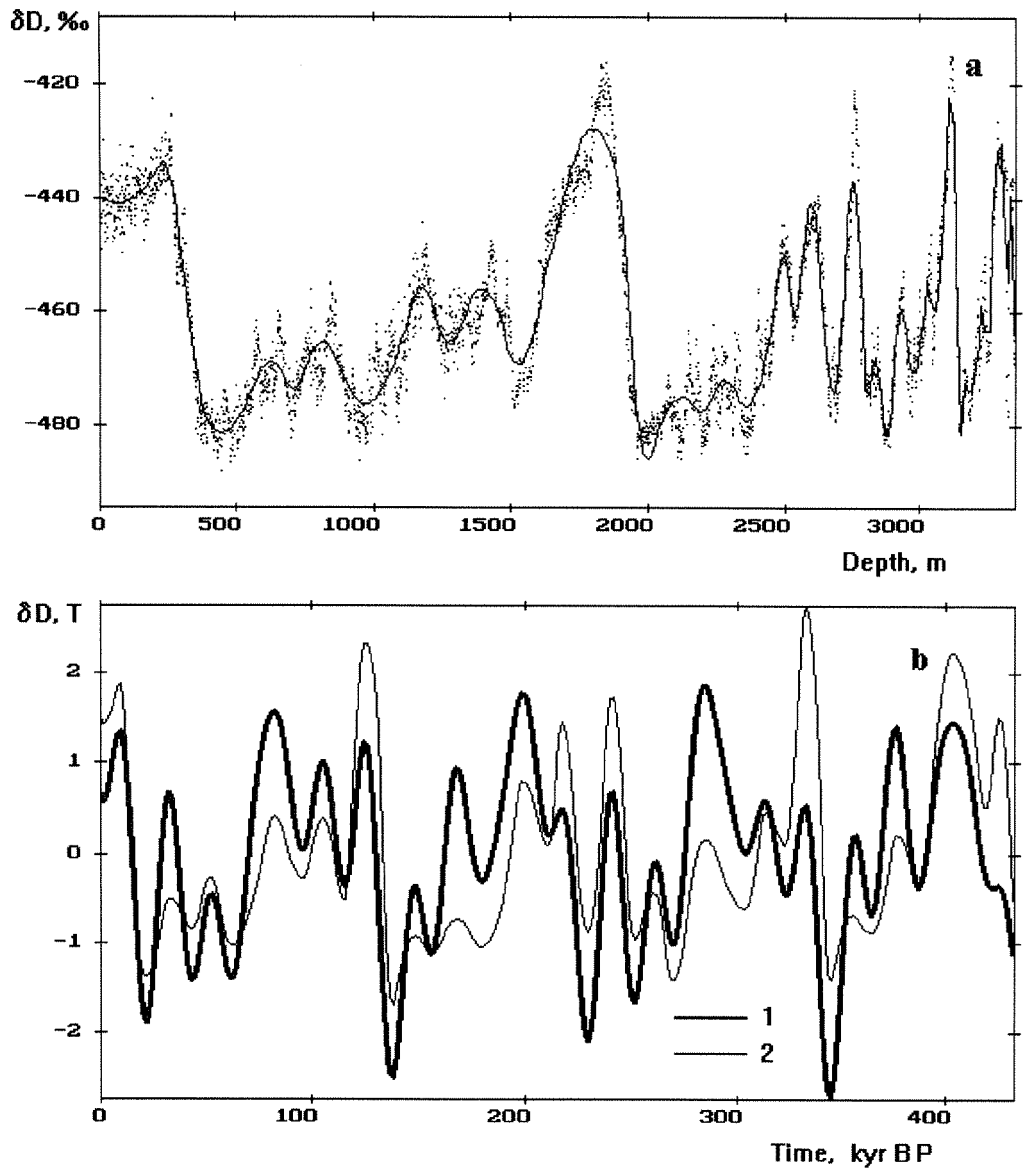


Figure 4: (**a**) Vostok deuterium ice core record (dots) and its parabolic-spline approximation (solid line) used in the ice-core age dating procedure. (**b**) The smoothed isotope record (curve 2) correlated with the metronome (curve 1) from Fig. 3a (both curves are normalized).

average standard error of the correlation is about 2.3 kyr. However, a special remark should be made here. Ice core analysis revealed [59] some indications of ice flow disturbances below 3310 m at Vostok. This considerably reduces the confidence in the identification and correlation of the two last extrema on the isotopic and metronomic signals in Fig. 4a. The corresponding ages are designated by "?" in Table 5.

A continuous time scale can be obtained by linear interpolation between neighboring points in Table 5. The normalized Milankovich component of the past

Table 5: Vostok ice core chronology. Age-depth correlation of peaks and troughs in metronomic and isotopic temperature signals and standard errors of the correlation.

| Depth, m | Age. kyr | Error kyr | Depth, m | Age, kyr | Error, kyr |
|---|---|---|---|---|---|
| 67 | 2.0 | 0.8 | 2678 | 229.6 | 1.1 |
| 233 | 9.6 | 0.9 | 2751 | 240.9 | 2.0 |
| 448 | 22.2 | 1.4 | 2810 | 251.7 | 1.8 |
| 623 | 33.0 | 2.5 | 2836 | 261.7 | 2.1 |
| 704 | 43.9 | 2.8 | 2876 | 270.0 | 3.6 |
| 811 | 52.8 | 2.6 | 2932 | 284.7 | 3.6 |
| 967 | 62.3 | 2.2 | 2975 | 304.2 | 1.9 |
| 1171 | 82.4 | 2.6 | 3029 | 313.2 | 2.3 |
| 1272 | 95.8 | 1.6 | 3050 | 323.6 | 1.4 |
| 1389 | 105.2 | 1.2 | 3110 | 332.4 | 1.4 |
| 1521 | 115.2 | 1.2 | 3153 | 344.8 | 1.4 |
| 1789 | 124.8 | 1.5 | 3168 | 356.6 | 2.1 |
| 2006 | 137.5 | 1.7 | 3186 | 364.4 | 1.4 |
| 2121 | 148.2 | 2.9 | 3231 | 375.6 | 2.9 |
| 2185 | 155.9 | 2.3 | 3248 | 386.7 | 4.9 |
| 2278 | 168.1 | 4.9 | 3291 | 403.0 | 4.5 |
| 2358 | 179.8 | 5.0 | 3323 | 419.5(?) | 2.0 |
| 2490 | 199.0 | 2.2 | 3335 | 426.3(?) | 2.7 |
| 2538 | 211.4 | 1.0 | 3350 | 434.6(?) | 4.2 |
| 2596 | 217.1 | 1.9 | — | — | — |

temperature variations on the ice sheet surface inferred from the borehole temperature profile and the smoothed ice core isotopic content fluctuations versus time are compared in Fig. 4b. In spite of the resemblance between the two curves, as before in [6], the difference mainly in the precession oscillations should be emphasized. In accordance with the sensitivity and resolution analyses performed in section 3, this discrepancy can be considered as a fact of a quantitative meaning only during the recent 20–40 kyr climate history.

The resulting Vostok timescale as a compound of linear interpolations is presented in Fig. 5 by the thick solid line. It closely coincides in its upper part with the timescale developed in [6] and does not noticeably differ from its preliminary version [7]. As before it is referred to as the Geophysical Metronome Timescale (GMTS). Again, we have to point out that the linear response of the climate to orbital forcing and the periodic extrapolation of Eq. 18 beyond the time range of the borehole temperature memory are the principal assumptions on which the formulation and the use of the metronome are based. Thus, additional error: ±2.5–3.5 kyr of the so-called overtuning effect [47–49] due to neglecting non-linearity in climatic transfer

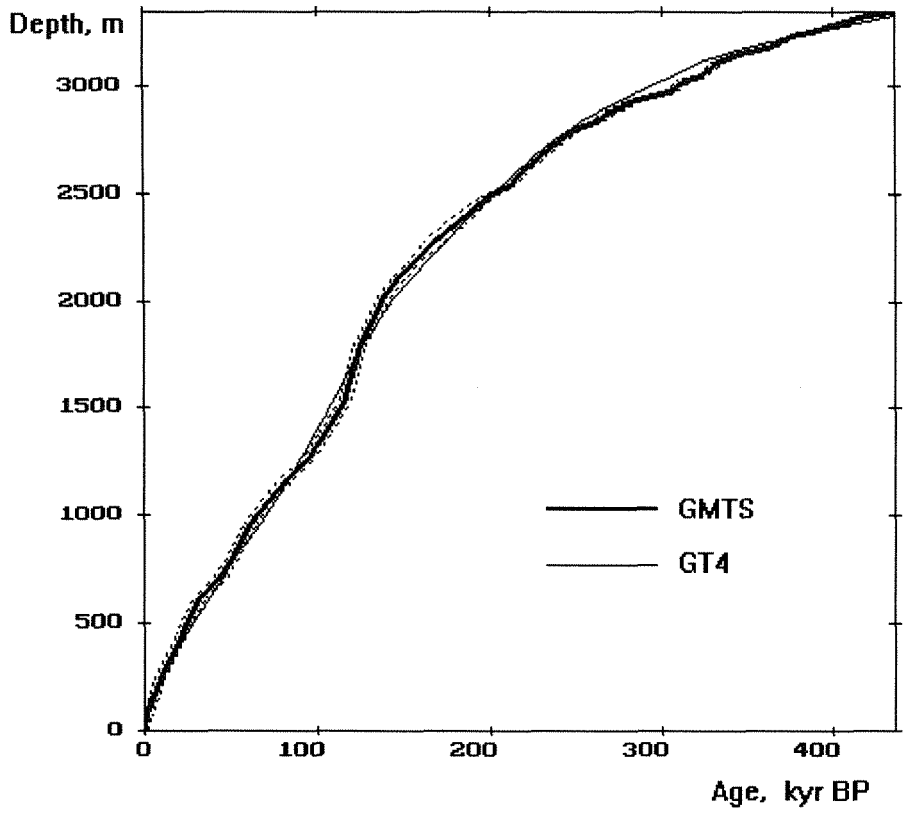


Figure 5: Age-depth relation for the Vostok ice core (GMTS) deduced from the analysis of the borehole temperature profile and its comparison with the glaciological timescale (GT4) developed on the basis of ice sheet flow modelling [59]. The error blanket indicates overall uncertainties of the GMTS chronology.

mechanisms should be taken into account. Combining the latter estimates with the standard correlation error, 2.3 kyr, we can predict the total average accuracy of the ice core chronostratigraphy (Table 5) as ±3.5–4.5 kyr. The distribution of the overall uncertainty of the dating along the Vostok ice core is shown in Fig. 5 as an error blanket by dotted lines.

Comparison of the upper part of GMTS down to 2755 m with different shallow timescales [31, 55, 71–73] and dust markers [56, 70] was discussed in details in [6]. It confirmed the validity of the dating procedure and the above estimates of its uncertainty. In Fig. 5, we compare GMTS with the new glaciological timescale GT4 [59] developed independently for Vostok on the basis of ice sheet dynamics computation. The standard deviation between the two chronologies is about 8.3 kyr which seems to be a rather good result if the above mentioned input-data problems of the direct ice flow modeling are taken into account. However the discrepancy reaches ±15–20 kyr in the deeper half of the ice core. The age of the ice at a depth of 3350 m predicted by GT4 (458.3 kyr) seems to be too large compared to 434.6 kyr of GMTS, although in the view of the above mentioned dynamic perturbations both estimates are not relevant.

Following Salamatin et al. [6], it is interesting to relate the events of the marine

stages in benthic $\delta^{18}O$ (global ice volume) variations and their ages [47, 48, 51] to those of the corresponding climatic changes revealed in the surface temperature variations at Vostok (see Fig. 3a and Table 5). This would result in the average lead of the polar temperature changes of about 2.9±3.4 kyr and 4.6±3.1 kyr for the dating [47, 48] and [51], respectively. Almost the same phase difference of 3±4 kyr in precession band was obtained in [55], and the phase lag estimate of 3–5 kyr between the benthic $\delta^{18}O$ signal and the southern sea surface temperatures was deduced in [57, 71]. A broad band phase lag centered on 2 kyr was found from the ice sheet modeling [77]. The above comparison confirms the expected consistency between GMTS and SPECMAP timescales.

### 4.2. Paleoclimatic reconstructions based on ice core isotope record

Let us now focus on the second problem of ice core data interpretation: conversion of the measured isotope records into past temperature changes. The conventional approach in this field is based on the use of Eqs. 19, 21 which were initially established as empirical geographical correlations for Antarctica [78, 79] and Greenland [80, 81] and reproduced by Raleigh-type modeling [62, 76]. The principal source of uncertainties here lies in the assumption that the local temporal and present-day spatial isotope-temperature relationships are identical [52, 80]. The GCM analysis [82] shows, for example, that for East Antarctica the difference may be of the order of 30 %. The recent rather exhaustive review [83] confirms the possibility of the temporal isotope-temperature slopes being up to 50 % less in comparison with their geographical analogues.

It is also very important to distinguish between the temperatures that are introduced and employed as paleoclimatic characteristics [25]. Ice core isotope records, for instance, are thought to represent climatic variations of the annual temperature in clouds where precipitation is formed, i.e. the averaged temperature at the top of inversion layer $T_i$ weighted by the subsidence seasonality effect [83]. The isotope-temperature ratio $C_T$ in Eq. 19 relates $\delta D$ to $\delta T_i$. On the other hand, the ice sheet body keeps memory about the past surface temperature $T_s$ in the upper stratum of snow-firn deposits where the boundary conditions on the glacier thermal state are imposed. As it has already been mentioned, it differs both from the surface-air temperature and from the inversion temperature. The total strength of inversion $T_i$–$T_s$ has a very specific seasonal nature [63, 64]. It reaches its maximum in winter, being close to zero in summer. Its magnitude is linked to the swing in seasonal surface temperatures. These temperatures, for instance, have much higher precession oscillations than annual temperatures in central Antarctica [65]. Thus, paleoclimatic changes in $T_s$ might not be merely proportional to $\delta T_i$, as it was predicted on geographical basis [62]. Eq. 19 and the use of the ratio $C_i$ most likely are valid for long-term climate variations but may fail in precession and shorter cycles. From this point of view borehole-temperature profiles could provide another unique piece of relevant information [1, 17, 36, 37, 40, 42, 84]. The studies [6, 36, 85–87] convincingly show the usefulness of borehole temperature for calibrating the isotopic paleothermometer.

It is important to recognize [6] that the primary step in matching the ice core isotopic ratios $\delta D$ with observed borehole temperature is to relate $\delta T_i$ to $\delta T_s$, which is the principal climatic input of the heat-and-mass-transfer model (13)–(16). Following [6], we assume a generalized form of the transfer function based on Eqs. 19, 21:

$$\delta T_s = \frac{\delta T_i}{C_i} - \frac{\alpha_{T_i} - \alpha_{T_s} C_i}{C_i}\left(K_i \delta\Delta - \alpha_L \delta^{18}O_{sw}\right) + \delta_p(t)$$

$$= \frac{\delta D - 8\delta^{18}O_{sw}}{C_i C_T} - \frac{\alpha_{T_i} - \alpha_{T_s} C_i}{C_i}\left(K_i \delta\Delta - \alpha_L \delta^{18}O_{sw}\right) + \delta_p(t). \quad (22)$$

Here $\alpha_{Ti}$ and $\alpha_{Ts}$ are the inversion and surface temperature-elevation gradients at the site of consideration; $\alpha_L$ relates sea level variations to the isotopic composition of sea water ($\alpha_L > 0$); $K_i$ is the isostasy coefficient approximately determined for ice-rock hydrostatic equilibrium as $K_i = 1 - \rho_0/\rho_r$, where $\rho_r$ is the density of rocks; $\delta\Delta = \Delta - \Delta^0$. The first leading term in Eqs. 22 is a direct consequence of Eqs. 19 and 21. The second term reflects the surface temperature variations induced by changes in the ice sheet surface elevation. It was estimated in [6] as being relatively small and insignificant. The principal innovation in Eqs. 22 is the introduction of a supplementary climatic signal $\delta_p(t)$ in $\delta T_s$ which does not exist in the scaled $\delta D$ (or $\delta T_i$) record, but might be remembered in the borehole temperature.

Now, when the ice core timescale is developed, another inversion problem can be formulated. The above parameterization (21), (22) of the past inversion and surface temperature variations can be constrained by the ice-sheet temperature memory at Vostok on the basis of the heat transfer and ice-flow model (13)–(16) and the target norm (20). As in [6], we assume $\alpha_{Ti} \approx \alpha_{Ts} \approx -0.01°C \cdot m^{-1}$ after [88], $\alpha_L \approx -100$ m·per mil$^{-1}$ after [89], and $K_i \approx 0.66$ ($\rho_0 = 920$ kg·m$^{-3}$, $\rho_r = 2700$ kg·m$^{-3}$). Consequently, $C_i$, $C_T$, and $\delta_p(t)$ are to be determined through minimization of the standard deviation $S$ between the simulated and observed borehole temperature profiles.

First of all the paleothermometer calibration was attempted in [6] at $\delta_p(t) \equiv 0$. In accordance with the structure of Eqs. 22, the product $C_i C_T$ was undoubtedly a single principal scaling parameter which influenced the $S$-function values. However, $C_T$ manifested itself additionally (although not dominantly) in accumulation rate predictions as a combination $C_T/\eta_b$ through Eqs. 14, 21. Conventional present-day geographical estimates of $C_T \approx 9$ per mil·°C$^{-1}$ and $C_i C_T \approx 6$ per mil·°C$^{-1}$ ($C_i \approx 0.67$) were confirmed as the best fit values but at a very high level of discrepancy between temperature measurements and computations: about 20 times greater than that for Milankovich metronome reconstructions. This was an evidence that additional $\delta_p$-signal did exist in the past surface temperature variations, but was missing in the scaled isotopic temperature record. The image of the signal kept in the borehole temperature memory, i.e. the difference between the measured temperature profile and its best-fit simulation, had a very close resemblance to what could have been induced in the ice sheet thickness by a supplementary precession cycle. We do not have sufficient direct information to extend $\delta_p$ periodically back into the past but the above mentioned

seasonal origin of the inversion strength could be one of the reasons for selective amplification of the precession climatic oscillations in the surface temperature which makes, in particular, the early Holocene temperatures warmer and the LGM temperatures colder in Antarctica than it was thought before. Certainly, this is not the only approach that might be considered and a borehole temperature profile could probably reveal more details in the recent paleotemperature history, but at least an additional precession signal $\delta_p$ (its recent period) is needed to correct the surface temperature variations $\delta T_s$ in Eqs. 22. Since climatic changes in the inversion and surface temperatures are assumed to be orbitally driven and synchronous, the inferable components of $\delta_p$ are taken after [6] proportional to the precession harmonics of the metronome given by Eq. 18:

$$\delta_p(t) = \alpha_p \sum_{i=3,4} [A_i \cos(\omega_i t) - B_i \sin(\omega_i t)], \quad -t_0 < t < 0, \qquad (23)$$

The inverse problem of the paleothermometer calibration is now formulated as a problem of the $S$-function minimization with respect to parameters $C_T$ and $\alpha_p$ for the stacked Vostok temperature profile at $C_i = 0.67$ and coefficients $A_i$, $B_i$ ($i$ = 3, 4), present-day surface temperature $T_s^0$, and geothermal flux $q_0$ taken as determined in section 3 in Milankovich metronome reconstructions (see Tables 3 and 4).

The best-fit values of the conversion parameters in Eqs. 22, 23, Holocene and LGM temperatures, and other estimates obtained for cases I (shear deformation and strain heating in the upper stratum of the ice sheet overlying the immovable bottom ice) and II (no shear in the freely floating ice) are brought together in Table 6. Time series of paleoclimatic characteristics inferred in case I are plotted in Fig. 6. The minimal standard deviations $S$ become comparable with those found for the metronomic signals, although the latter ones still remain twice as small, since the paleothermometer parameterization in the form of Eqs. 22, 23 is not so flexible as that of Eq. 18. This confirms the above supposition that a more accurate temperature profile might be used in future to achieve a higher resolution of the LGM–Holocene climate at Vostok.

The primary result of the reconstruction is that the introduction of an additional precession signal in the surface temperature variations noticeably improves the fit between the simulated and measured temperature profiles and leads to 50 % lower estimates of the temporal deuterium-temperature slopes in comparison with their spatial values. Both $C_i$ and the product $C_i C_T$ in Eqs. 22 should be considered now as scaling parameters relative to the long-term climate variations only. The annual temperature on the ice sheet surface and the inversion strength undergo more intensive and selectively amplified oscillations in the precession band with additional increase in their amplitudes of about 1.5–2.0°C represented by the $\delta_p$ signal. This implies that the recent glacial-interglacial temperature transition over central Antarctica deduced from the stacked borehole temperature profile at Vostok could be even greater than it was predicted in [6]. The LGM–Holocene temperature increase was about 20–23±3°C in the ice sheet temperature and about 13–15°C in the inversion temperature (see Table 6 and Fig. 6a, curves 1, 3). The surface temperature reconstruction performed in this section on the basis of the ice core isotope

record appears to be rather close to the metronomic signal (compare curves 1 and 2 in Fig. 6a), especially during the recent 25-kyr interval of the borehole temperature memory. All estimates of the LGM surface temperature presented in Tables 4 and 6 agree within the uncertainties predicted by the Monte Carlo resolution analysis. However, the paleothermometer calibration is thought to be more reliable.

Interpretations of the GISP2 [86] and GRIP [87] ice core isotope records using borehole thermometry revealed similar changes (21–22°C) in the surface temperature in central Greenland. It should be emphasized once more that, as against the unique situation in Antarctica, the long term (obliquity and eccentricity) climatic cycles can not be separately distinguished in the borehole temperature and the paleothermometer calibration procedure could not have felt the selective amplification of the precession signal even if it had existed in the Greenland inversion strength in the past. Recent direct paleotemperature reconstruction [42] predict somewhat larger glacial-interglacial increase in the surface temperature over central Greenland: 24.5±2°C. Additional argument for a higher estimate of the LGM-to-Holocene warming in Antarctica could be obtained from the analysis of crystal growth in the ice sheet [90]. Recent ice core isotope measurements at Low Dome (Antarctica) and their comparison with measured temperature seasonality [91] have also shown that the temporal oxygen isotope-temperature gradient is about 40 % less than the estimate based on the local spatially derived calibration. In the coastal region (with minimal strength of the inversion) the last glaciation has been predicted to be ~13°C colder than present. This finding agrees well with the inferred inversion temperature change at Vostok.

Table 6: Results of isotopic paleothermometer calibration at Vostok.

| **Parameters, characteristics** | **Case I** | **Case II** |
|---|---|---|
| Precession amplification factor: | | |
| $\alpha_p$ | 0.24 | 0.31 |
| $\delta D/\delta T_i$ temporal slope: | | |
| $C_T$, per mil·°C$^{-1}$ | 4.9 | 4.3 |
| $\delta D/\delta T_s$ long-term temporal slope: | | |
| $C_i C_T$, per mil·°C$^{-1}$ | 3.3 | 2.9 |
| Mean surface temperature: | | |
| $\langle T_s \rangle$, °C | −65.5 | −66.2 |
| Holocene-optimum surface temperature, °C | −53.9 | −53.0 |
| LGM surface temperature, °C | −74.2 | −76.3 |
| Standard deviation: | | |
| $S$, °C | 0.026 | 0.015 |

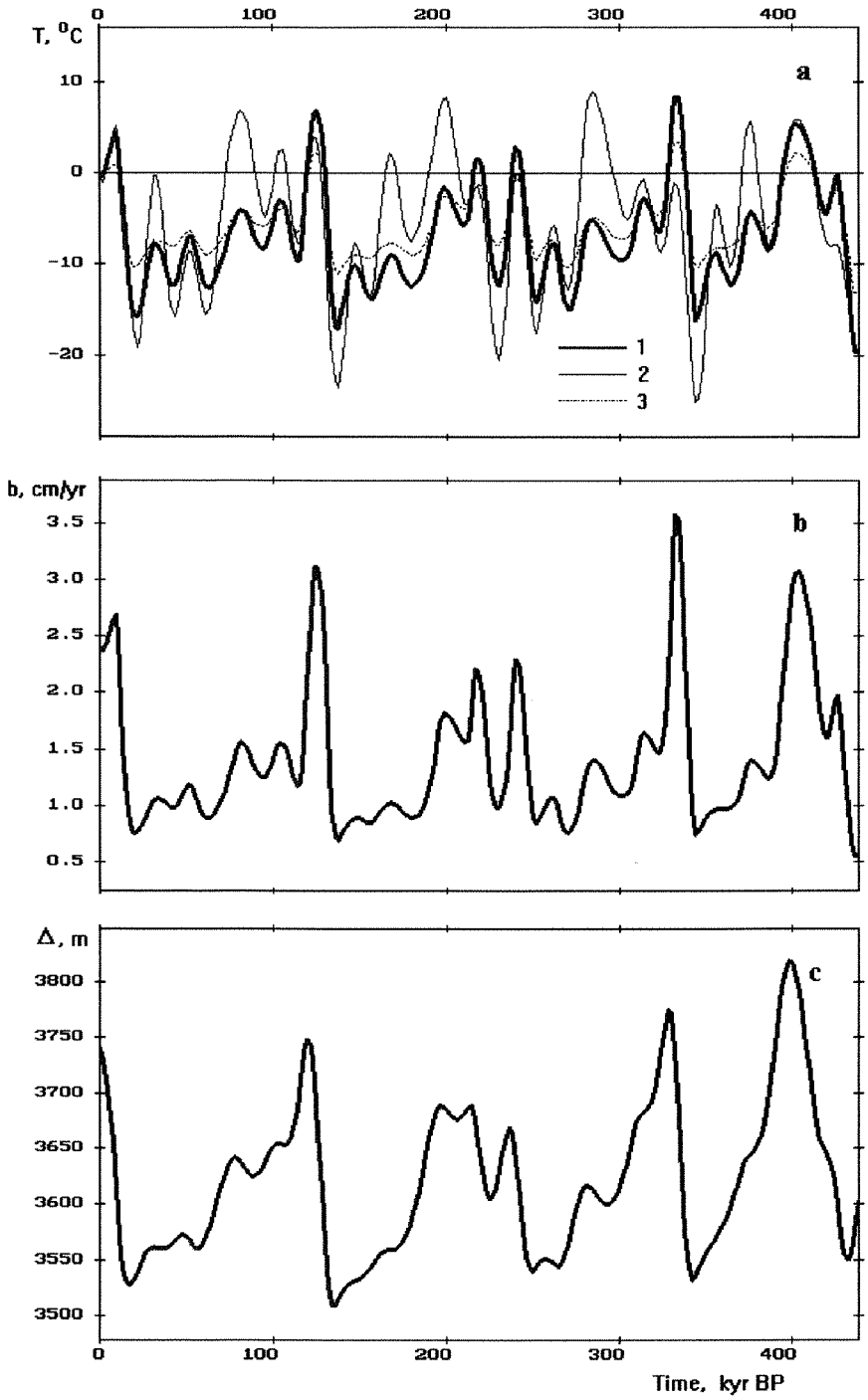


Figure 6: Time series of paleoenvironmental characteristics reconstructed from the smoothed Vostok isotope record for case I with the shear deformation and strain heating in the 3540-meter stratum of the ice sheet overlying the immovable ice. (**a**) Temperature variations on the ice sheet surface (curve 1) and inversion temperature oscillations (curve 3) counted from their present-day reference levels in comparison with the Milankovich metronomic signal (curve 2). (**b**) Accumulation rate variations calculated from inversion temperatures. (**c**) Past changes in the ice-sheet thickness simulated at Vostok.

Past variations of the accumulation rate $b$ and ice sheet thickness $\Delta$ (in ice equivalent) are simulated simultaneously with the paleothermometer calibration on the basis of the climatic submodel (14), (15). The new peculiarities in the isotope record interpretation lead to new predictions of their changes which directly depend on $\delta T_i$ and hence on the factor $C_T$. Figs. 6b and 6c show the accumulation-rate and ice-sheet-thickness fluctuations at Vostok in the past for case I but do not differ much from those in case II. The general picture remains close to the earlier reconstructions [6, 7]. The maximal swing of the ice thickness oscillations between glacial and interglacial stages might reach 200–250 m.

### 4.3. Summary of glaciological implications

The stacked temperature profile measured in the 3623-meter deep borehole at Vostok Station provides an important additional constraint for ice core dating and isotopic paleothermometer calibration. The extended Geophysical Metronome Timescale (GMTS) is deduced by correlating the major climatic events in the smoothed isotopic temperature record with those in the local geophysical metronome inferred from the borehole temperature memory as a dominant Milankovich component of the past temperature variations on the glacier surface. The total accuracy of the ice core chronology is estimated to be about ±3.5–4.5 kyr on average. The age of ice at the end of the isotope record, at a depth of 3350 m, is predicted as 434.6 kyr. GMTS, based on the general tuning approach, is thought to be consistent with the SPECMAP chronologies established for deep-sea records.

The conversion procedure of matching the scaled isotope (deuterium) record to the temperature profile at Vostok revealed relatively more intensive (additionally amplified) precession oscillations in surface temperatures than in inversion temperature fluctuations. The total surface temperature increase during the last deglacial transition is found now to be almost two times higher than it was predicted from contemporary spatial isotope-temperature correlations in Antarctica. The mean Pleistocene-climate temperature on the glacier surface at Vostok is estimated as $\langle T_s \rangle \approx -66$°C and is about 7–8°C lower than its present-day value $T_s^0 = -58.4$°C. The surface temperature increased from −75±3°C in the LGM at 22 kyr BP to its Holocene maximum −53.5±1°C at 9.6 kyr BP. Past variations of the accumulation rate and the corresponding changes in the ice-sheet surface elevation are simultaneously simulated.

## 5. Conclusion

The paper continues the research line started in [4–7]. It is mainly a review, but it also contains new results and revises previous studies. The paper does not cover all details of paleoclimatic reconstructions discussed earlier in [1–7]. On the other hand, for the first time, it summarizes and presents the complete description of the model on which the Vostok borehole thermometry interpretations were and are based. The stacked, recently extended, 3600-meter deep borehole temperature profile [7] is used now for ice core dating and paleoclimatic analysis. A Monte Carlo random walk method has additionally been introduced into computational experiments to estimate the uncertainty of the inverse problem solutions. The principal results and

conclusions are outlined as summaries at the end of each section.

Here, we would like to emphasize that the studies performed in this paper confirm or detail all earlier findings. They show that the borehole temperature memory in central part of the Antarctic ice sheet, in particular at Vostok, contains unique data on the past climate changes and on the thermal conditions in the basal stratum (subglacial lake). More accurate temperature measurements are needed to achieve a better resolution of the recent LGM-Holocene climate history. Paleotemperatures inferred at present can be considered as a background for future reconstructions.

## Acknowledgements

The study presented in this paper has more than ten-year history. This work would not have been possible without continuous and close collaboration between the Department of Applied Mathematics of Kazan State University and the Department of Drilling Technics and Technologies (the Laboratory of Antarctic Research) of St. Petersburg Mining Institute initiated by B. B. Kudryashov in 1973. The drilling team from the laboratory has carried out all thermal and mechanical drilling operations at Vostok Station, the geophysicists have performed all temperature surveys in the deep boreholes. It is a great pleasure to work with these people and I am grateful to V. K. Chistyakov, R. N. Vostretsov, D. N. Dmitriyev, K. V. Blinov, N. V. Vasilyev, Yu. Rydvan, and A. Volkov for their cooperation and for providing the borehole thermometry data. This project is also a total of long collaborative activities of the Department of Applied Mathematics and Arctic and Antarctic Research Institute in the field of polar ice sheet modeling and paleoreconstructions. I am especially thankful to N.I. Barkov and V.Ya. Lipenkov for their direct participation in this study, numerous fruitful discussions, and assistance. Most of the principal results reviewed here or continued in the newly performed computational experiments were obtained in the Laboratory of Glaciology and Geophysics of Environment (Grenoble, France) together with J. Jouzel, J.R. Petit, D. Raynaud, and C. Ritz. I should express my special gratitude to them as well as to C. Lorius, P. Duval, C. Waelbroeck, for their support, important comments, and stimulating criticism. From the very beginning the main idea of the project was appreciated and the research was supported from Hokkaido University by S. Mae and T. Hondoh. Thanking them for their interest to this work, I would like to emphasize the role of T. Hondoh, as the Head of the ICSI Working Group on Physics of Ice-Core Records (PICR), in selecting and promoting this topic as an invited talk at the PICR International Symposium (14-17 September, 1998, Shikotsukohan, Japan). During this meeting and at earlier stages, the study has gained much from useful discussions with J.M. Barnola, T. Blunier, W.F. Budd, G. Clow, K.M. Cuffey, D. Dahl-Jensen, V.M. Kotlyakov, A.J. Payne, B. Stauffer, Ed. Waddington, and O. Watanabe.

This collaborative work was supported by the European Science Foundation through the European Ice Sheet Modellng Initiative programme, by the USA National Science Foundation (Office of Polar Programs, Antarctic Sciences Section), and by the Ministry for General and Professional Education and by the State Committee for

Science and Technologies of the Russian Federation.

## References

1. N.I. Barkov, K.V. Blinov, V.N. Petrov, and A.N. Salamatin, Chislennyye eksperimenty po rekonstruktsii paleoklimata na osnove rezul'tatov termometrii glubokoy skvazhiny na stantsii Vostok v Antarktide [Numerical experiments on paleoclimate reconstructions from temperature measurements in the deep borehole drilled in the ice sheet at Vostok Station, Antarctica], *Mater. Glyatsiol. Issled.*, **67**, 116-121 (1989).
2. A.N. Salamatin, Ice sheet modeling taking account of glacier ice compressibility, *Glacier-Ocean-Atmosphere Interactions*, *International Association of Hydrological Sciences Publ. 208*, 183-192 (1991).
3. A.N. Salamatin, V.Ya. Lipenkov, and K.V. Blinov, Vosstanovleniye klimaticheskih izmeneniy temperatury na poverhnosti antarkticheskogo lednikovogo pokrova v proshlom po resul'tatam temperaturnih izmereniyi v glubokih skvazhinah na stantsii Vostok [Reconstruction of temperature climatic variations on the Antarctic ice sheet in the past from temperature measurements in deep bore-holes at Vostok Station], *Mater. Glyatsiol. Issled.*, **79**, 59-64 (1995) [Translation in: *Mater. Glyatsiol. Issled.*, **81** (IAHS Symp. at Tashkent 1993 – Seasonal and Long-term Fluctuations of Nival and Glacial Processes in Mountains at Different Scales of Analysis), 141-146 (1997)].
4. A.N. Salamatin, V.Ya. Lipenkov, and K.V. Blinov, Vostok (Antarctica) climate record time-scale deduced from the analysis of a borehole-temperature profile, *Annals of Glaciology*, **20**, 207-214 (1994).
5. A.N. Salamatin and C. Ritz, A simplified multi-scale model for predicting climatic variations of the ice sheet surface elevation in the Central Antarctica, *Annals of Glaciology*, **23**, 28-35 (1996).
6. A.N. Salamatin, V.Ya. Lipenkov, N.I. Barkov, J. Jouzel, J.R. Petit, and D. Raynaud, Ice core age dating and paleothermometer calibration based on isotope and temperature profiles from deep boreholes at Vostok Station (East Antarctica), *J. Geophys. Res.*, **103**(D8), 8963-8977 (1998).
7. A.N. Salamatin, R.N. Vostretsov, J.R. Petit, V.Ya. Lipenkov, and N.I. Barkov, Geophysical and paleoclimatic implications of the stacked temperature profile from the deep borehole at Vostok Station (Antarctica), *Mater. Glyatsiol. Issled.*, **85**, 233-240 (1998).
8. A.N. Salamatin, Vzaimodeystviye temperaturnih i gidrodinamicheskih poley v statsionarnih kupolovidnih lednikah [The interaction of temperature and hydrodynamic fields in stationary dome-like glaciers], *Mater. Glyatsiol. Issled.*, **42**, 122-128 (1981).
9. V.Yu. Potapenko and A.N. Salamatin, Kriterialniy analiz uravneniy opisyvayuschih termodinamicheskiye protsessy v lednikovih pokrovah [The similarity analysis of equations governing thermal and dynamic processes in ice sheets], *Problemy Arktiki i Antarktiki*, No.50, 74-77 (1985).

10. V.Ya. Lipenkov, A.N. Salamatin, and P. Duval, Bubbly-ice densification in ice sheets: II. Applications, *J. Glaciol.*, **43**(145), 397-407 (1997).
11. P.V. Hobbs, *Ice Physics*, Oxford, Clarendon Press (1974).
12. R.N. Vostretsov, D.N. Dmitriyev, O.F. Putikov, K.V. Blinov, and S.V. Mitin, Osnovnyye rezul'taty geofizicheskikh issledovaniy glubokikh skvazhin i ledyanogo kerna v Vostochnoy Antarktide [The main results of geophysical studies of deep boreholes and the ice core in East Antarctica], *Mater. Glyatsiol. Issled.*, **51**, 172-178 (1984).
13. M. Sturm, J. Holmgren, M. König, and K. Morris, The thermal conductivity of seasonal snow, *J. Glaciol.*, **43**(143), 26-41 (1997).
14. C. Ritz, Time dependent boundary conditions for calculation of temperature fields in ice sheets, *The Physical Basis of Ice Sheet Modeling, International Association of Hydro-logical Sciences Publ. 170*, 208-216 (1987).
15. D. Dahl-Jensen, N.S. Gundestrup, K. Keller, S.J. Johnsen, S.P. Gogineni, C.T. Allen, T.S. Chuah, H. Miller, S. Kipfstuhl, and E.D. Waddington, A search in north Greenland for a new ice-core drill site, *J. Glaciol.*, **43**(144), 300-306 (1997).
16. A.N. Salamatin, Tri mesyatsa v institute nizkotemperaturnih issledovaniy (Universitet Hokkaido, Sapporo, Yaponiya) [Three months in the Institute of Low Temperature Science (Hokkaido University, Sapporo, Japan)], *Mater. Glyatsiol. Issled.*, **83**, 227-230 (1997).
17. C. Ritz, Interpretation of the temperature profile measured at Vostok. East Antarctica, *Annals of Glaciology*, **12**, 138-144 (1989).
18. A.P. Kapitsa, J.R. Ridley, G de Q. Robin, M.J. Siegert, and I.A. Zotikov, A large deep freshwater lake beneath the ice of central East Antarctica, *Nature*, **381**, 684-686 (1996).
19. L. Lliboutry, How to model the waxing and waning of ice-sheets, *GeoResearch Forum Vols. 3-4 (Dynamics of the Ice Age Earth: A Modern Perspective)*, 249-270 (1998).
20. A.M. Popkov, G.A. Kudryavtsev, S.R. Verkulich, V.N. Masolov, and V.V. Lukin, Seismic studies in the vicinity of Vostok Station (Antarctica), *Lake Vostok Study: Scientific Objectives and Technological Requirements.* Abstracts of the International Workshop (March 24-26, 1998, Arctic and Antarctic Research Institute, St.Petersburg, Russia), 26-27 (1998).
21. V.Ya. Lipenkov and N.I. Barkov, Internal structure of the Antarctic ice sheet as revealed by deep core drilling at Vostok Station, *Lake Vostok Study: Scientific Objectives and Technological Requirements.* Abstracts of the International Workshop (March 24-26, 1998, Arctic and Antarctic Research Institute, St. Petersburg, Russia), 31-35 (1998).
22. J.R. Petit, I. Basile, J. Jouzel, N.I. Barkov, V.Ya. Lipenkov, R.N. Vostretsov, N.I. Vasiliev, and C. Rado, Preliminary investigations and implications from the 3623 m Vostok deep ice core studies, *Lake Vostok Study: Scientific Objectives and Technological Requirements.* Abstracts of the International Workshop (March 24-26, 1998, Arctic and Antarctic

Research Institute, St. Petersburg, Russia), 43-44 (1998).

23. L. Lliboutry, A critical review of analytical approximate solutions for steady state velocities and temperatures in cold ice-sheets, *Z. Gletscherkd. Glazialgeol.*, **15**(2), 135-148 (1979).
24. C. Ritz, *Un modèle thermo-mecanique d'évolution pour le bassin glaciaire Antarcique Vostok-glacier Byrd: sensibilité aux valeurs des paramèters mal connus*, (Thése de Doctorat d'Etat) Université Joseph Fourier - Grenoble I, L.G.G.E. (1992).
25. G.de Q. Robin, Ice cores and climatic change, *Phil. Trans. R. Soc. Lond.*, **B.280**, 143-168 (1977).
26. N.I. Barkov and V.Ya. Lipenkov, Nakopleniye snega v rayone stantsii Vostok, Antarktida, v 1970-1992 gg. [Snow accumulation at Vostok Station, Antarctic, 1970-1992], *Mater. Glyatsiol. Issled.* **80**, 87-88 (1996).
27. A.C. Fowler and D.A. Larson, On the flow of polythermal glaciers. I: Model and preliminary analysis, *Proc. R. Soc. London, Ser. A*, **343**(1713), 217-242 (1978).
28. A.N. Salamatin, Analiz prosteyshih matematicheskih modeley kupolovidnih lednikov [Analysis of the simplest mathematical models of dome-shaped glaciers], *Issled. Prikladnoy Matematike*, **7**, 131-139 (1979) [Translation in *J. Sov. Math.*, **43**(3), 2506-2512 (1988)].
29. A.N. Salamatin and A.B. Mazo, Issledovaniye obschey matematicheskoy modeli kupolovidnogo lednika metodami teorii podobiya [Similarity analysis of the general mathematical model of an ice-cap glacier], *Issled. Prikladnoy Matematike*, **10**, 139-149 (1984) [Translation in *J. Sov. Math.*, **44**(5), 664-672 (1989)].
30. D.J. Drewry (Ed.), *Antarctica: glaciological and geophysical folio*, Cambridge, Scott Polar Research Institute (1983).
31. J. Jouzel, N.I. Barkov, J.M. Barnola, M. Bender, J. Chappellaz, G. Genton, V.M. Kotlyakov, V. Lipenkov, C. Lorius, J.R. Petit, D. Raynaud, G. Raisbeck, C. Ritz, T. Sowers, M. Stievenard, F. Yiou and P. Yiou, Extending the Vostok ice-core record of paleoclimate to the penultimate glacial period. *Nature*, **364**(6436), 407-412 (1993).
32. W.F. Budd, The dynamics of ice masses. *ANARE Sci. Rep.* 108 (1969).
33. K.M. Cuffey and G.D. Clow, Temperature accumulation, and ice sheet elevation in central Greenland through the last deglaciation transition. *J. Geophys. Res.*, **102**(C12), 26,383-26,396 (1997).
34. A.L. Berger, Long-term variations of daily insolation and quaternary climatic changes, *J. of Atmospheric Sciences*, **35**, 2362-2367 (1978).
35. C. Ritz, L. Lliboutry and C. Rado, Analysis of 870 m deep temperature profile at Dome C, *Annals of Glaciology.*, **3**, 284-289 (1982).
36. W.F. Budd and N.W. Young, Application of modelling techniques to measured profiles of temperatures and isotopes, In: *The Climatic Record in Polar Ice Sheets*, 150-177, G. de Q. Robin (Ed.), Cambridge University Press, New York (1983)
37. D. Dahl-Jensen and S.J. Johnsen, Paleotemperatures still exist in the Greenland ice sheet, *Nature*, **320**(6059), 250-252 (1986).

38. J. Firestone, *Resolving the Younger Dryas Event through Borehole Thermometry* (Ph.D. Dissertation), Univ. of Washington, Geophysics Program (1992).
39. V. Rommelaere, *Trois Problèmes Inverses en Glaciologie* (Thèse de Doctorat), Université Joseph Fourier - Grenoble I, L.G.G.E. (1997).
40. T. Lewis (Ed.), Climatic change inferred from underground temperatures (special issue), *Palaeogeogr., Palaeoclimatol., Palaeoecol. (Global and Planetary Change Section)*, **98**(2/4) (1992).
41. D.R. MacAyel, J. Firestone, and Ed. Waddington, Paleothermometry by control methods, *J. Glaciol.*, **37**(127), 326-338 (1991).
42. D. Dahl-Jensen, K. Mosegaard, N. Gundestrup, G.D. Clow, S.J. Johnsen, A.W. Hansen, and N. Balling, Past temperatures directly from the Greenland ice sheet, *Science*, **282**, 268-271 (1998).
43. D. Dahl-Jensen, S.J. Johnsen, W.S.B. Paterson, and C. Ritz, Comments on "Paleothermometry by control methods" by MacAyel and others, *J. Glaciol.*, **39**(132), 421-423 (1993).
44. D.R. MacAyel, J. Firestone, and Ed. Waddington, Paleothermometry redux, *J. Glaciol.*, **39**(132), 423-431 (1993).
45. K. Mosegaard and A. Tarantola, Monte Carlo sampling of solutions to inverse problems, *J. Geophys. Res.*, **100**(B7), 12,431-12,447 (1995).
46. K. Mosegaard, Resolution analysis of general inverse problems through inverse Monte Carlo sampling, *Inverse Problems*, **14**, 405-426 (1998).
47. J. Imbrie, J.D. Hays, D.G. Martinson, A. McIntyre, A.C. Mix, J.J. Morley, N.G. Pisias, W.L. Prell, and N.J. Shackleton, The orbital theory of Pleistocene climate: support from a revised chronology of the marine $\delta^{18}O$ record, *Milankovich and Climate, Part 1*, 269-305, A.L. Berger et al. (Eds.), D. Reidel Publishing Company (1984).
48. D.G. Martinson, N.G. Pisias, J.D. Hays, J. Imbrie, T.C. Moore, and N.J. Shackleton, Age dating and the orbital theory of ice ages: development of a high-resolution 0 to 300,0000-year chronostratigraphy, *Quaternary Research*, **27**(1), 1-29 (1987).
49. J. Imbrie, E.A. Boyle, S.C. Clemens, A. Duffy, W.R. Howard, G. Kukla, J. Kutzbach, D.G. Martinson, A. McIntyre, A.C. Mix, B. Molfino, J.J. Morley, L.C. Peterson, N.G. Pisias, W.L. Pell, M.E. Raymo, N.J. Shackleton, and J.R. Toggweiler, On the structure and origin of major glaciation cycles. 1. Linear responses to Milankovich forcing, *Paleoceanography*, **7**(6), 707-738 (1992).
50. J. Imbrie, A. Berger, E.A. Boyle, S.C. Clemens, A. Duffy, W.R. Howard, G. Kukla, J. Kutzbach, D.G. Martinson, A. McIntyre, A.C. Mix, B. Molfino, J.J. Morley, L.C. Peterson, N.G. Pisias, W.L. Pell, M.E. Raymo, N.J. Shackleton, and J.R. Toggweiler, On the structure and origin of major glaciation cycles. 2. The 100,000-year cycle, *Paleoceanography*, **8**(6), 707-738 (1993).
51. F.C. Bassinot, L.D. Labeyrie, E. Vincent, X. Quidelleur, N.J. Shackleton, and Y. Lancelot, The astronomic theory of climate and the age of the Bruhes-Matuyama magnetic reversal, *Earth and Planetary Science Letters*, **126**, 91-108 (1994).

52. C. Lorius, J. Jouzel, C. Ritz, L. Merlivat, N.I. Barkov, Y.S. Korotkevich, and V.M. Kotlyakov, A 150,000 year climatic record from Antarctic ice, *Nature*, **316**(6029), 591-596 (1985).
53. J. Jouzel, C. Lorius, J.R. Petit, C. Genton, N.I. Barkov, V.M. Kotlyakov, and V.M. Petrov, Vostok ice-core: A continuous isotope temperature record over the last climatic cycle (160,000 years), *Nature,* **329**(6138), 403-408 (1987).
54. C. Genton, J.M. Barnola, D. Raynaud, C. Lorius, J. Jouzel, N.I. Barkov, Y.S. Korotkevich and V.M. Kotlaykov, Vostok ice-core: climatic response to $CO_2$ and orbital forcing changes over the last climatic cycle, *Nature*, **329**(6138), 414-418 (1987).
55. C. Waelbroeck, J. Jouzel, L. Labeyrie, C. Lourius, M. Labracherie, M. Stievenard and N.I. Barkov, Comparing the Vostok ice deuterium record and series from Southern Ocean core MD 88-770 over the last two glacial-interglacial cycles, *Climate Dynamics*, **12**, 113-123 (1995).
56. J. Jouzel, C. Waelbroeck, B. Malaize, M. Bender, J.R. Petit, M. Stievenard, N.I. Barkov, J.M. Barnola, T. King, V.M. Kotlyakov, V. Lipenkov, C. Lorius, D. Raynaud, C. Ritz, and T. Sowers, Climatic interpretation of the recently extended Vostok ice records, *Climate Dynamics*, **12**, 513-521 (1996).
57. L. Labeyrie, M. Labracherie, N. Gorfti, J.J. Pichon, M. Vautravers, M. Arnold, J.C. Duplessy, M. Paterne, E. Michel, J. Duprat, M. Caralp, and J.L. Turon, Hydrographic changes of the Southern Ocean (southeast Indian sector) over the last 230 kyr, *Paleoceanography*, **11**(1), 57-76 (1996).
58. J.R. Petit, I. Basile, A. Leruyuet, D. Raynaud, C. Lorius, J. Jouzel, M. Stievenard, V.Ya. Lipenkov, N.I. Barkov, B.B. Kudryashov, M. Davis, E. Saltzman, and V. Kotlyakov, Four climate cycles in Vostok ice core, *Nature*, **387**, 359-360 (1997).
59. J.R. Petit, J. Jouzel, D. Raynaud, N.I. Barkov, J.M. Barnola, I. Basile, M. Bender, J. Chappellaz, J. Davis, G. Delaygue, M. Delmotte, V.M. Kotlyakov, M. Legrand, V.Ya. Lipenkov, C. Lorius, L. Pepin, C, Ritz, E. Saltzman, and M. Stievenard, Climate and atmospheric history of the past 420,000 years from the Vostok ice core, Antarctica, *Nature*, **399**, 429-436 (1999).
60. S.J. Johnsen, H.B. Clausen, W. Dansgaard, N.S. Gundestrup, C.U. Hammer, U. Anderson, K.K. Anderson, C.S. Hvidberg, D. Dahl-Jensen, J.P. Steffensen, H. Shoji, A.E. Sveinbjörnsdóttir, J. White, J. Jouzel, and D. Fisher, The $\delta^{18}O$ record along the Greenland Ice Core Project deep ice core and the problem of possible Eemian climatic instability, *J. Geophys. Res.*, **102**(C12), 26,397-26,410 (1997).
61. P. Yiou, K. Fuhrer, L.D. Meeker, J. Jouzel, S. Johnsen, and P.A. Mayewski, Paleoclimatic variability inferred from the spectral analysis of Greenland and Antarctic ice-core data, *J. Geophys. Res.*, **102**(C12), 26,441-26,454 (1997).
62. J. Jouzel and L. Merlivat, Deuterium and oxygen 18 in precipitation: modeling of the isotopic effects during snow formation, *J. Geophys. Res.*, **89**(D7), 11,749-11,757 (1984).

63. W.M. Connolley, The Antarctic temperature inversion, *Int. J. Climatology*, **16**, 1333-1342 (1996).
64. H.R. Phillpot and J.W. Zillman, The surface temperature inversion over the Antarctic continent, *J. Geophys. Res.*, **75**(21), 4161-4169 (1970).
65. D.A. Short, J.G. Mengel, T.J. Crowley, W.T. Hyde, and G.R. North, Filtering of Milankovich cycles by Earth's geography, *Quaternary Research*, **35**, 157-173 (1991).
66. M.J. Siegert and J.A. Dowdeswell, Spatial variations in heat at the base of the Antarctic ice sheet from analysis of the thermal regime above subglacial lakes, *J. Glaciol.*, **42**(142), 501-509 (1996).
67. W. Dansgaard, S.J. Johnsen, H.B. Clausen, D. Dahl-Jensen, N.S. Grundestrup, C.U. Hammer, C.S. Hvidberg, J.P. Steffensen, A.E. Svelnbjornsdottlr, J. Jouzel, and G. Bond, Evidence for general instability of past climate from a 250-kyr ice-core record, *Nature*, **364**(6434), 218-220 (1993).
68. R.B. Alley, C.A. Shuman, D.A. Meese, A.J. Gow, K.C. Taylor, K.M. Cuffey, J.J. Fitzpatrick, P.M. Grootes, G.A. Zielinski, M. Ram, G. Spinelli, and B. Elder, Visual-stratigraphic dating of the GISP2 ice core: Basis, reproducibility, and application, *J. Geophys. Res.*, **102**(C12), 26,367-26,381 (1997).
69. D.A. Meese, A.J. Gow, R.B. Alley, G.A. Zielinski, P.M. Grootes, M. Ram, K.C. Taylor, P.A. Mayewski, and J.F. Bolzan, The Greenland Ice Core Project 2 depth-age scale: Methods and results, *J. Geophys. Res.*, **102**(C12), 26,411-26,423 (1997).
70. J.R. Petit, L. Mounier, J. Jouzel, Y.S. Korotkevich, V.M. Kotlyakov, and C. Lorius, Paleo-climatological and chronological implications of the Vostok core dust record, *Nature,* **343**(6253), 56-58 (1990).
71. J.-J. Pichon, L.D. Labeyrie, G. Bareille, M. Labracherie, J. Durpat, and J. Jouzel, Surface water temperature changes in the high latitudes of the southern hemisphere over the last glacial - interglacial cycle, *Paleoceanography*, 7, 289-318 (1992).
72. N. Shackleton, J. Le, A. Mix, and M.A. Hall, Carbon isotope records from Pacific surface waters and atmospheric carbon dioxide, *Quat. Sci. Rev.*, **11**, 387-400 (1992).
73. T. Sowers, M. Bender, L. Laberyrie, D. Martinson, J. Jouzel, D. Raynaud, J.J. Pichon, and Y.S. Korotkevich, A 135,000-year Vostok-SPECMAP common temporal framework, *Paleoceanography,* **8**(6), 737-766 (1993).
74. J.M. Barnola, P. Pimienta, D. Raynaud, and Y.S. Korotkevich, $CO_2$-climate relationship as deduced from the Vostok ice-core: A re-examination based on new measurements and on a revaluation of the air dating, *Tellus,* **43B**, 83-90 (1991).
75. T. Sowers, M. Bender, D. Raynaud, and Y.S. Korotkevich, The $\delta^{15}N$ of $N_2$ in air trapped in polar ice: A tracer of gas transport in the firn and a possible constraint on ice age - gas age difference, *J. Geophys. Res.,* **97**(D14), 15,683-15,697 (1992).
76. W. Dansgaard, Stable isotopes in precipitation, *Tellus*, **16**, 436-468 (1964).
77. W.F. Budd and P. Rayner, Modelling ice sheet and climate changes through

the ice ages, NATO ASI Series, Vol. **I 12**, *Ice in the Climate System* (Ed. W. Richard Peltie), Springer-Verlag Berlin Heidelberg, 291-319, (1993).

78. C. Lorius and L. Merlivat, Distribution of mean surface stable isotope values in East Antarctica: observed changes with depth in the coastal area, *Isotopes and Impurities in Snow and Ice. International Association of Hydrological Sciences Publ. 118*, 127-137 (1977).
79. Q. Dahe, J.R. Petit, J. Jouzel, and M. Stievenard, Distribution of stable isotopes in surface snow along the route of the 1990 International Trans-Antarctica Expedition, *J. Glaciol.*, **40**(134), 107-118 (1994).
80. W. Dansgaard, S.J. Johnsen, H.B. Clausen, C.U. Hammer, and N. Grundestrup, Stable isotope glaciology, *Meddelesser om Greenland*, **197**(2), 1-53 (1973).
81. S. Johnsen, W. Dansdaard, and J.W.C. White, The origin of Arctic precipitation under present and glacial conditions, *Tellus*, **41B**, 452-468 (1989).
82. J. Jouzel, R.D. Koster, R.J. Suozzo, and G.L. Russell, Stable water isotope behavior during the last glacial maximum: A GCM analysis, *J. Geophys. Res.*, **99**(D12), 25,791-25,801 (1994).
83. J. Jouzel, R.B. Alley, K.M. Cuffey, W. Dansgaard, P. Grootes, G. Hoffmann, S.J. Johnsen, R.D. Koster, D. Peel, C.A. Shuman, M. Stievenard, M. Stuiver, and J. White, Validity of temperature reconstruction from water isotopes in ice cores, *J. Geophys. Res.*, **102**(C12), 26,471-26,487 (1997).
84. G.de Q. Robin, Reconciliation of temperature-depth profiles in polar ice sheets with surface temperatures deduced from oxygen-isotope profiles, *J. Glaciol.*, **16**(74), 9-22 (1976).
85. K.M. Cuffey, R.B. Alley, P.M. Grootes, J.M. Bolzan, and S. Anandakrishnan, Calibration of the $\delta^{18}O$ isotopic paleothermometer for central Greenland, using bore hole temperatures, *J. Glaciol.*, **40**(135), 341-349 (1994).
86. K.M. Cuffey, G.D. Clow, R.B. Alley, M. Stuiver, Ed.D. Waddington, and R.W. Saltus, Large Arctic temperature change at the Glacial-Holocene transition, *Science*, **270**, 455-458 (1995).
87. S. Johnsen, D. Dahl-Jensen, W. Dansgaard, and N. Grundestrup, Greenland palaeo-temperatures derived from GRIP borehole temperature and ice-core isotope profiles, *Tellus*, **47B**(5), 624-629 (1995).
88. V.G. Aver'yanov, Gradienty temperatury vozduha u poverhnosty lednikovogo pokrova Antarktidy [Air temperature gradients at the Antarctic ice-sheet surface], In: *Geograficheskiye i glyatsiologicheskiye issledovaniya v polyarnikh stranakh*, 55-60, Leningrad: Gidrometeoizdat, (1988).
89. M.L. Prentice, L.D. Meeker, and P.A. Mayewski, Links between fast changes in sea level, ice-sheet volume, and climate, *J. Geophys. Res.* (in press).
90. J.R. Petit, P.Duval, and C. Lorius, Long-term climatic changes indicated by crystal growth in polar ice, *Nature*, **326**(6108), 62-64 (1987).
91. T.D. van Ommen and V. Morgan, Calibrating the ice core paleothermometer using seasonality, *J. Geophys. Res.*, **102**(D8), 9351-9357 (1997).